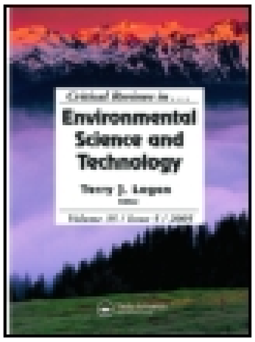

Critical Reviews in Environmental Science and Technology

ISSN: 1064-3389 (Print) 1547-6537 (Online) Journal homepage: https://www.tandfonline.com/loi/best20

Remotely assessing and monitoring coastal and inland water quality in China: Progress, challenges and outlook

Yujiu Xiong, Yili Ran, Shaohua Zhao, Huan Zhao & Qixuan Tian

CRITICAL REVIEWS IN ENVIRONMENTAL SCIENCE AND TECHNOLOGY
https://doi.org/10.1080/10643389.2019.1656511

Remotely assessing and monitoring coastal and inland water quality in China: Progress, challenges and outlook

Yujiu Xiong[a,b], Yili Ran[c], Shaohua Zhao[d], Huan Zhao[d], and Qixuan Tian[e]

[a]School of Civil Engineering, Sun Yat-sen University, Guangzhou, Guangdong, China; [b]Guangdong Engineering Technology Research Center of Water Security Regulation and Control for Southern China, Sun Yat-sen University, Guangzhou, Guangdong, China; [c]School of Geography and Planning, Sun Yat-sen University, Guangzhou, Guangdong, China; [d]Satellite Environment Center, Ministry of Ecology and Environment/State Environmental Protection Key Laboratory of Satellite Remote Sensing, Beijing, China; [e]School of Geographical Sciences, Taiyuan Normal University, Taiyuan, Shanxi, China

ABSTRACT

China faces increasingly serious water scarcity due to the uneven distribution of available water resources, rapid economic development, and water pollution. The current war on water pollution by the Chinese government requires nationwide water quality information at high spatiotemporal resolution that can be obtained by only remote sensing (RS) methods. However, it is challenging to remotely retrieve such information from turbid Case-2 waters. This paper reviews four aspects of the major achievements in remotely sensed coastal and inland water quality in China. Specifically, achievements in atmospheric correction prior to water quality retrieval, progress in water-related sensor design, developments (improvements) to existing Case-2 water algorithms, and advances in oil spill and harmful algal bloom monitoring. Major challenges are identified, including: 1) a large mismatch exists between the water quality information required and RS datasets due to a lack of professional inland water sensors; 2) planned monitoring and field experiments for studying the optical properties of inland waters are scarce; and 3) RS of urban black odorous waters and international rivers is of great urgency. This review may provide scientific guidelines for obtaining information about coastal and inland waters and assist water resource managers and aquatic ecologists in controlling water pollution.

KEYWORDS

Water quality; remote sensing; Case-2 water; spatial resolution; temporal resolution; China

1. Introduction

Fresh water is a crucial resource for humans (Wada, Wisser, & Bierkens, 2014) and other life on Earth (Van Dijk et al., 2013). However, fresh water accounts for only 2.5% of the global water, and the amount of available

CONTACT Shaohua Zhao zshyytt@126.com Satellite Environment Center, Ministry of Ecology and Environment/State Environmental Protection Key Laboratory of Satellite Remote Sensing, Beijing, 100094, China.
Color versions of one or more of the figures in the article can be found online at www.tandfonline.com/best.

water is even less due to its uneven distribution (Oki & Kanae, 2006). Many of these waterbodies, such as inland rivers and lakes, have been altered and threatened by intensive human activities (Vörösmarty et al., 2010). As such, water quality and quantity, which are two attributes that determine water availability, exhibit large spatial differences depending on the levels of water withdrawal, consumption, wastewater discharge, and pollution.

As a rapidly developing country, China is facing increasingly serious water scarcity due to the uneven distribution of water resource availability and ongoing demands for water (Liu & Yang, 2012; Jiang, 2015; Cai et al., 2019). It has been reported that China's annual per capita availability of renewable water resources (approximately 2100 m^3) is less than one-third of the world average (CAE, 2000; Jiang, 2015; FAO, 2019). Taking Beijing in arid North China and Shenzhen and Guangzhou in humid coastal regions as examples, the mean multiyear amounts of available water resources per person were approximately 140, 170 and 520 m^3, respectively.

In addition to physical and economic water scarcity, water contamination has exacerbated the shortage of water resources across China (Tao & Xin, 2014; Han, Currell, & Cao, 2016; Wang, Li, Li, Kharrazi, & Bai, 2018). According to statistics released by the Ministry of Environmental Protection (MEP), the water quality of one quarter of the seven major river basins in China is unsuitable for direct human contact (classified as IV or worse, see Table A1 for detailed definitions) (Figure 1). Approximately 40% of other types of surface water, i.e. lakes and reservoirs, have exhibited poor water quality (class IV or worse) in the last 15 years (Figure 1), and this deterioration in water quality has been significantly accelerated by nitrogen pollution and eutrophication (Gao et al., 2019). Similarly, 27% of China's near coastal waters are classified as poor (class IV or worse, see Table A1 for details) (Figure 1). Due to the limited number of monitoring sites (or the limited monitoring ability), the degree of water pollution at the national scale is likely worse than indicated by the assessments based on the above statistics because small rivers or tributaries with serious pollution levels were excluded from these evaluations (Han et al., 2016).

Under the impacts of increasing occurrence of extreme weather events (i.e. droughts and floods) (e.g. Xu, Milliman, & Xu, 2010), the number of waterbodies with poor water quality has increased (e.g. Paerl & Huisman, 2009; Chapra et al., 2017), particularly lakes and reservoirs in urban areas (e.g. Deng, Zhang, Qin, Yao, & Deng, 2017, Deng et al., 2018; Zhang, Shi, et al., 2018). Water pollution not only threatens water security and aggravates the water crisis in China (Lu et al., 2015; Jiang, 2015; Han et al., 2016) but also causes diseases and threatens public health (Zhang et al., 2010; Gong et al., 2012; Tao & Xin, 2014). The management of water pollution in China is urgent, and therefore, water resource managers in

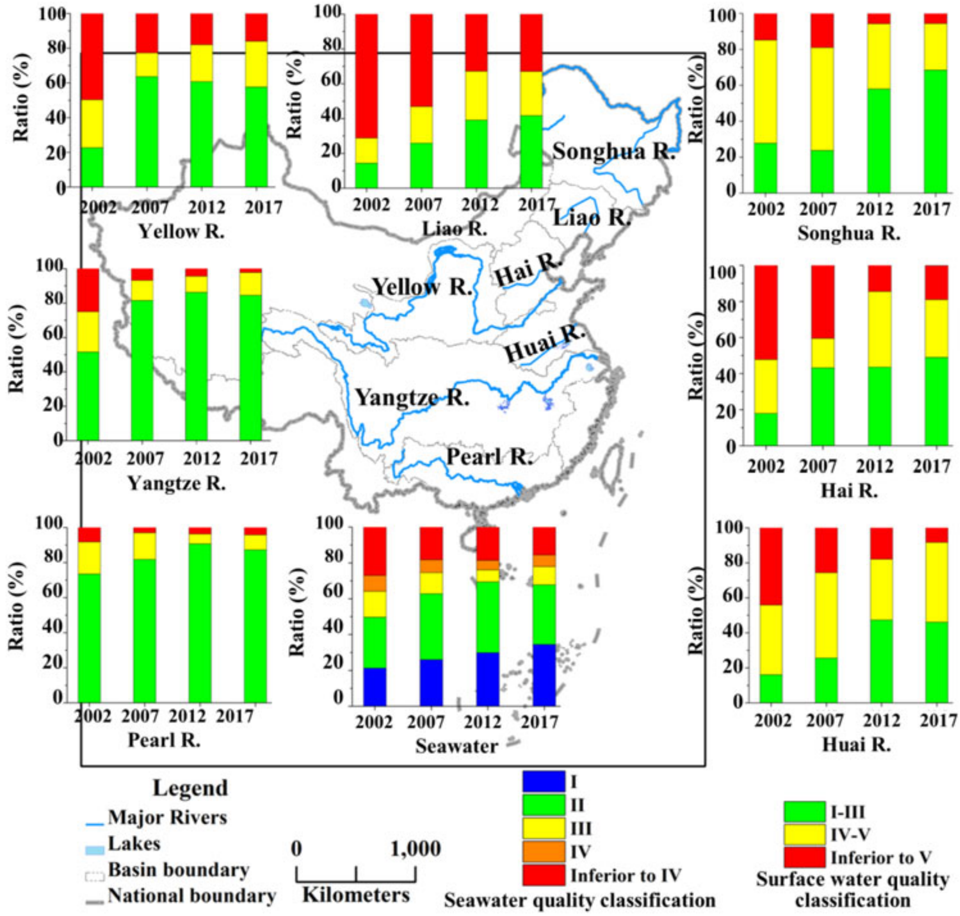

Figure 1. Surface water quality of the seven major river basins and nearshore coastal waters in China based on decadal government statistics. Note: water quality decreases as the Roman numerals change from I to V; the surface water quality was classified according to environmental quality standards for surface water (GB3838-2002), whereas the coastal waters was classified according to the sea water quality standard (GB3097-1997) and specification for offshore environmental monitoring (HJ 442-2008).

the Chinese government require detailed and periodic water quality information.

Remote sensing (RS), which detects a target by measuring its electromagnetic radiation (ER) without contacting the target directly, is recognized as the most suitable and economical way of providing periodic and spatially continuous information for evaluating and monitoring water quality (e.g. Chang, Imen, & Vannah, 2015; Mouw et al., 2015; Dörnhöfer & Oppelt, 2016). Reliable water quality information from RS data benefits water resource management and the development of mitigation measures. For example, founded in 2009 by the MEP, the Satellite Environment Center (SEC) is responsible for monitoring environmental-related parameters, including water quality, and offers crucial technological support to the

MEP for managing water environments (Zhao et al., 2017). However, due to the complicated optical properties of waterbodies, especially inland waterbodies, the use of RS to assess water quality remains challenging. Therefore, the objectives of this paper were to 1) provide an update on the studies on RS-based water quality assessments and monitoring in China and 2) identify the current challenges and opportunities (or possible solutions) for future studies as well as water resource management.

2. Theory for the RS of water quality

This section briefly describes the basic theory of using RS to assess water quality. Figure 2a shows a simplified schematic of solar radiation transfer and its interaction with the atmosphere, water, and sensors. In pure water, most light is generally absorbed, and the light penetration depth in the open ocean is much deeper than that in coastal waters (Figure 2b). The optical properties of the open ocean (Case-1 waters) are mainly dominated by phytoplankton that absorb light and ocean color, and phytoplankton are represented by the chlorophyll-a concentration (Chla) (Behrenfeld, Boss, Siegel, & Shea, 2005), which is relatively easy to retrieve. However, coastal and inland waters are generally turbid (Case-2 waters), and contain other optically active constituents in addition to phytoplankton, i.e. inorganic suspended particulate matter (SPM) and colored dissolved organic matter (CDOM), which have absorption spectra similar to Chla (Gordon & Morel, 1983). When water quality retrieval methods based on Case-1 waters are applied in turbid inland and coastal Case-2 waters, they may fail due to significant

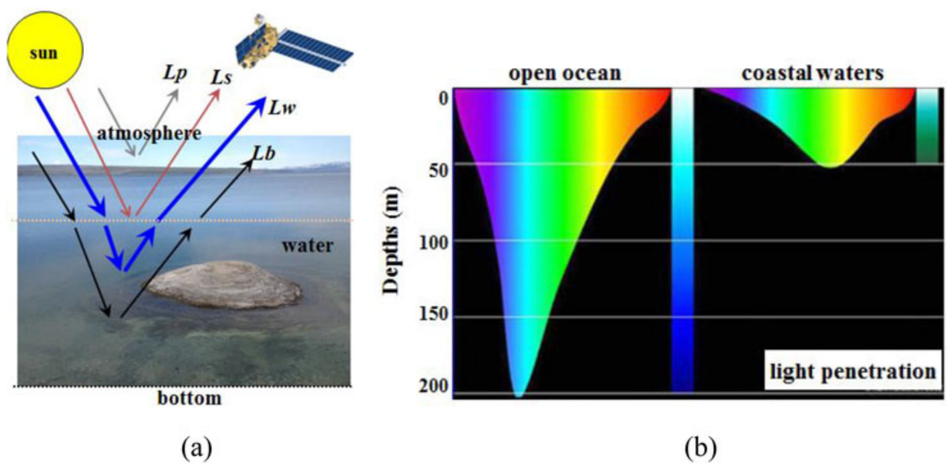

Figure 2. Light and water: (a) a schematic map showing the radiance received by a sensor system over water; (b) light penetration ability in two different water types. Note: L_p, L_s, L_w, and L_b in panel (a) represent atmospheric path radiance, free-surface layer reflected radiance, subsurface water-leaving radiance, and bottom reflected radiance, respectively; panel (b) is cited from Hollocher (2002).

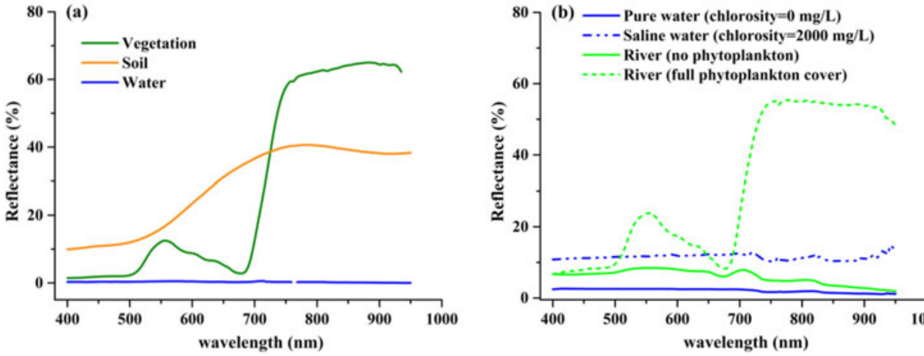

Figure 3. Spectral characteristics of water: (a) comparison of spectral reflectance among water, vegetation, and soil; (b) comparison of spectral reflectance between different inland waters. Note: the vegetation and soil datasets were cited from the spectral library (Kokaly et al., 2017), and the other data were measured using FieldSpec 3 (ASD Inc., USA). The blue lines in panel (b) were measured under controlled experiments at the south campus of Sun Yat-Sen University on July 23, 2011, and the green lines were measured at Wenyu River, Beijing on June 16, 2007.

differences in optical properties. In addition, the amount of energy reflected by waterbodies is relatively small compared to that reflected by soil and vegetation (Figure 3a). Even similar waterbodies with different chlorosity values (or different amounts of phytoplankton cover) exhibit different amounts of energy reflection (Figure 3b). In this case, limited ER is reflected back to the sensors, which results in challenges in interpreting the spectral signals.

Nonetheless, the scientific community has remotely estimated the quality of Case-2 waters by unremitting efforts using indices, such as Chla, CDOM, and total suspended matter (TSM), as summarized in Odermatt, Gitelson, Brando, and Schaepman (2012), Chang et al. (2015), Mouw et al. (2015), and Palmer, Kutser, and Hunter (2015). These indices are related to the recorded spectral signal that is backscattered from water through empirical or analytical models (Figure 4), as follows (Schmugge, Kustas, Ritchie, Jackson, & Rango, 2002):

$$Y = A + BX \ \ or \ \ Y = AB^X \tag{1}$$

where Y is the water quality index (e.g. Chla or TSM) and X is the signal recorded by RS (e.g. radiance), which can be from a single band or a combination of bands (e.g. band ratio). A and B are the coefficients.

For empirical methods, A and B are often determined via the relationship between the sampled water quality index and RS data (e.g. Carpenter & Carpenter, 1983). Although empirical methods with simple computation requirements are easy to apply and can offer effective evaluation (Matthews, 2011), such algorithms are limited to applications in certain areas and times because coefficients are derived from site-specific samples (IOCCG, 2000). Later, the understanding of the relationship between light,

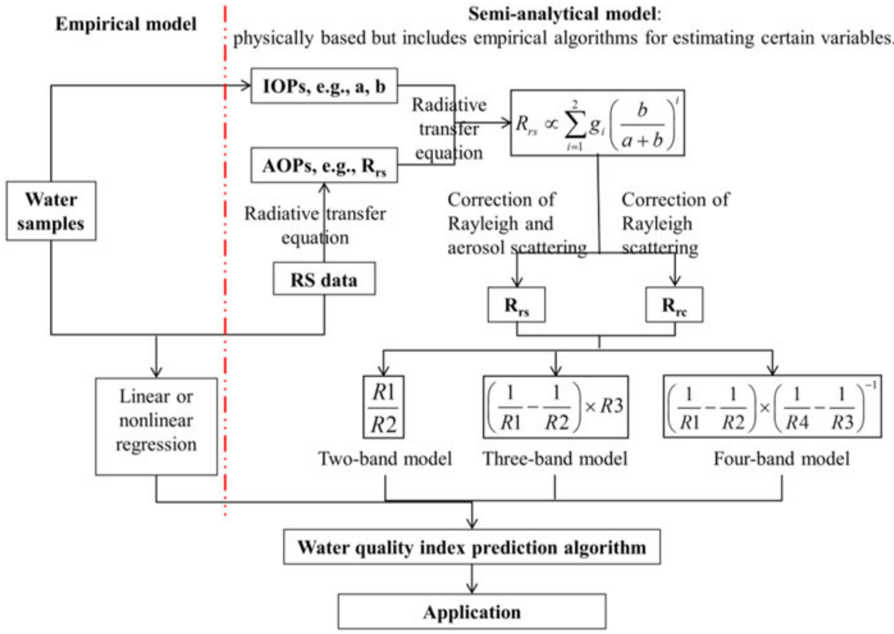

Figure 4. Simplified schematic relationship between the water quality index and RS. Note: apparent and inherent optical properties (AOPs and IOPs) are correlated by the radiative transfer equation; the relationship between R_{rs} and absorption and scattering coefficients (i.e. a and b) is simplified based on the radiative transfer equation; g is geometrical factor; R is reflectance of band i.

the atmosphere, and water constituents (that influence water quality) was improved. Specifically, it was found that apparent optical properties (AOPs) of water, such as the RS reflectance just below the water surface (R_{rs}), depend on both the medium and the directional structure of the ambient light field, whereas inherent optical properties (IOPs), i.e. absorption and the scattering coefficients, depend on only the medium (Ogashawara, 2015 and references therein). Therefore, bio-optical models based on radiative transfer theory have been used to quantify the relationship between IOPs and AOPs and then relate various water quality indices to the corresponding water constituents (IOCCG, 2000; Ogashawara, Mishra, & Gitelson, 2017).

3. Recent advances in remotely sensed water quality in China

Currently, remotely sensed water quality indices mainly include Chla, CDOM, TSM, Secchi disk depth (Z_{SD}), and euphotic zone depth (Z_{eu}) as well as parameters indicating optical properties, e.g. R_{rs}, the absorption coefficient (a), and the scattering coefficient (b). In addition to these indices, some other indices required in water resource management are also assessed and monitored in China, such as total phosphorus (TP), total nitrogen (TN), dissolved oxygen (DO), biochemical oxygen demand (BOD), and chemical oxygen demand (COD). In this study, rather than providing an exhaustive review of the water quality of inland and coastal waters determined by RS in China, we mainly focus on the following crucial achievements.

3.1. Advances in atmospheric correction prior to water quality retrieval

Atmospheric correction is crucial for quantitative RS (Liang, 2004), and accurate atmospheric correction for obtaining R_{rs} is technically challenging for turbid inland waters because RS signals may contain a large amount of noise or may be saturated (Li, Hu, et al., 2017). In ocean color studies, the purpose of atmospheric correction is to remove noise resulting from absorption (by gases and aerosols) and scattering (by air molecules and aerosols). Atmospheric correction is commonly based on dark objects under the assumption that seawater absorbs all light in the red and near-infrared (NIR) spectral bands (i.e. L_w =0). However, while the theory can be accurately applied in the open ocean, considerable bias is generated when applying atmospheric correction to turbid coastal and inland waters because scattering is enhanced by particles, and dark objects may disappear.

To address this challenge, Wang and Shi (2007) proposed an atmospheric correction method by combining MODIS NIR and shortwave infrared (SWIR) bands. This method was shown to exhibit reasonable accuracy in retrieving the L_w in turbid coastal waters along the east China. Later, Wang, Shi, and Tang (2011) further improved the SWIR-based atmospheric correction method for the highly turbid Lake Taihu and generated high-quality L_w data. Recently, to utilize low-quality MODIS-Terra data for inland waters, Li, Hu, et al. (2017) proposed a recovery method via noise reduction and calibration-based atmospheric correction. The authors found that the accuracy was significantly improved by applying the method over turbid Lake Taihu and Lake Chaohu. The abovementioned methods can fully remove the noise contributed by both Rayleigh and aerosol scattering. If Rayleigh correction is simplified, e.g. allowing for the existence of aerosol contributions, the impact of land adjacency effects on small waterbodies in middle-lower Yangtze River lakes and the Yangtze River Estuary could be addressed, thus increasing the amount of usable MODIS data (Feng, Hou, Li, & Zheng, 2018).

An additional challenge in atmospheric correction for coastal and inland waters is sunglint correction, especially for RS data with a relatively high spatial resolution (e.g. decameter-scale pixels compared to kilometer-scale pixels) (Harmel, Chami, Tormos, Reynaud, & Danis, 2018). Sunglint refers to the intensive reflection of solar radiation from a water surface. Figure 5

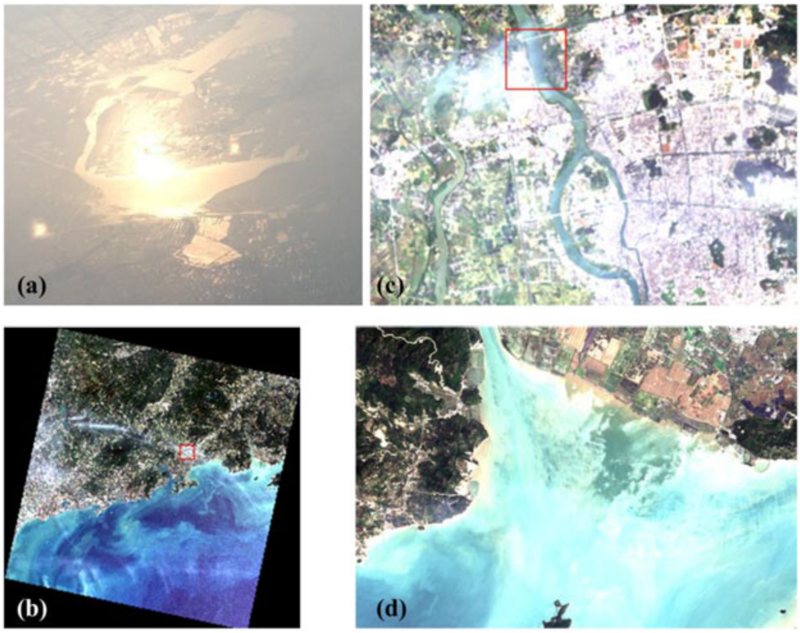

Figure 5. Sunglint and its impact on RS imagery: (a) a photo taken from a plane; (b) a Landsat 8 false-color image (RBG = 432, path 123 and row 45) of the coastal areas and adjacent regions of Yangjiang city in Guangdong Province scanned on April 8, 2018; (c) and (d) are selected examples of sunglint from (b) for an inland river and a river outlet, respectively.

shows examples of sunglint contamination on waterbodies, which lowers the signal of RS data. Studies on sunglint correction are limited (Kay, Hedley, & Lavender, 2009; Kutser, Vahtmäe, & Praks, 2009; Martin, Eugenio, Marcello, & Medina, 2016; Harmel et al., 2018), and no related work has been reported in China.

3.2. Advances in water quality retrieval

Substantial progress has been made in water quality RS in China, although most of these studies have depended on data from international satellites due to the relatively limited development of domestic satellites (see Section 3.3 for details). Tables 1 to 3 list the major RS-retrieved water quality indices, and the three indices that mostly influence water optical properties (i.e. Chla, CDOM, and SPM) were analyzed as follows.

3.2.1. Chla

The Coastal Zone Color Scanner (CZCS) was launched in 1978 (Gordon et al., 1983), and this satellite sensor was the first designed for mapping global ocean surface Chla. Later, a second generation of ocean color satellite missions began operating in the late 1990s (IOCCG, 1999), including

Table 1. Historical ocean-color sensors used to remotely assess and monitor inland and coastal water qualities in China.

Sensor	Platform	Swath (km)	Spatial resolution (m)	Water quality index (range)	Algorithm and band(s) used	Performance (R^2)	Study area	Reference
CZCS	Nimbus-7 (USA)	1556	825	Pigment (0.04–9 mg m^{-3})	OC3: 443, 520, 550 nm	—	Chinese coastal waters	Tang, Ni, Muller-Karger, & Oh, 2004
CMODIS	SZ-3 (China)	650–700	400	SSC(∼0–1000 mg L^{-1})	Empirical: 550, 670 nm	0.91	Yangtze River Estuary	Han et al., 2006
HICO	ISS (USA)	50	100	Chla (0.11–582 mg m^{-3})	Empirical GABI: 443, 490, 555, 680, 709 nm	0.94	Yangtze River Estuary†	Shanmugam et al., 2018
					OC2: 488, 547 nm	0.73		
					OC3: 443, 486, 551 nm	0.72		
					OC4: 443, 490, 510, 555 nm	0.68		
					Red-NIR: 665 nm	0.78		
					Red-NIR: 665, 708, 753 nm	0.63		
				SPM(0.675–25.7 mg L^{-1})	Empirical: 555, 645nm	0.88	Pearl River Estuary	Zhao et al., 2018
MERIS	ENVISAT (Europe)	1150	300/1200	Chla(30–130 mg m^{-3}),	SAMO-LUT: 665, 709, 754 nm	0.76	Lake Dianchi	Yang et al., 2011
				CDOM(0.4–1.75 m^{-1})	SAMO-LUT: 560, 665 nm	0.21		
				Chla (5.5–64.8 mg m^{-3})	Cluster-based red-NIR: 665, 709, 754 nm	0.79	Lake Taihu	Shi et al., 2013
				Chla (0.7–12 mg m^{-3})	Empirical NGRDI: 560, 681 nm	0.71	Lake Poyang	Feng, Hu, Han, Chen, & Qi, 2014
				Chla (5.0–77.5 μg L^{-1})	Empirical: 560, 665, 681, 709 nm	0.57	Lake Taihu	Zhang et al., 2019
					Hard-classification based: 665, 709 (or 560, 681; 681, 709) nm	0.73		
					Soft-classification based: 665, 709 (or 560, 681; 681, 709) nm	0.81		
				Cyanobacterial PC (1.6–263.7 μg L^{-1})	Semi-analytical PCI: 560, 620, 665 nm	0.64	Lake Taihu	Qi et al., 2014
				Cyanobacteria abundance (5–100 %)	Empirical: 560, 620, 665, 681, 709 nm	0.92	Lakes Taihu and Chaohu	Jin et al., 2017
				Cyanobacterial bloom or floating leaf	Empirical CSI (+PCI): 681, 754 nm	—	Lake Taihu	Zhu, Li, Zhang, & Shen, 2018
				POC (0.8–33.4 mg L^{-1})	Semi-analytical: 665, 754, 779 nm	0.51	Lake Taihu	Lyu, Wang, Jin, Shi, et al., 2017
				POC(17.6–687.5 mg m^{-3})	Empirical: 443, 555 nm	0.53	South China Sea	Hu et al., 2016
SeaWiFs	OrbView-2 (USA)	2806	1100	Chla(0.04–10 mg m^{-3})	OC4: 443, 490, 510, 555 nm	0.85	Yellow River Estuary	Wu et al., 2016
				Chla(0.5–10 mg m^{-3})	Empirical (+ OC3): 412, 443, 490, 555 (443, 490, 555) nm	0.53	Bohai Sea	Zhang, Qiu, Sun, Wang, & He, 2017
				Chla (0.02–8.34 mg m^{-3})	Modified OC4: 412, 443, 490, 555 nm	0.63	Yellow and East China Seas	Siswanto et al., 2011
				TSM (0.04–340 mg m^{-3})	Empirical: 490, 555, 670 nm	0.90		
				CDOM (0.5–34.3 cm^{-1})	Empirical: 443, 490, 555 nm	0.71		
				POC(17.6–687.5 mg m^{-3})	Empirical: 443, 555 nm	0.72	South China Sea	Hu et al., 2016
				TSM(0.4–1143 g m^{-3})	Empirical: 7 bands from 402 to 785 nm	0.91	East China Sea	Mao, Chen, Pan, Tao, & Zhu, 2012

Note: CDOM represented by its absorption coefficient at 440 nm; †Datasets are not from only the Yangtze River Estuary.

Table 2. Current dedicated ocean-color sensors used to remotely assess and monitor inland and coastal water qualities in China.

Sensor	Platform	Swath (km)	Spatial resolution (m)	Water quality index (range)	Algorithm and band(s) used	Performance (R^2)	Study area	Reference
GOCI	COMS (South Korea)	2500	500	Chla (5.58–185.3 μg L^{-1})	Empirical: 680, 745 nm	0.75	Lake Taihu	Du et al., 2017
				TP (0.02–0.367 mg L^{-1})	Empirical: 412, 865 nm	0.72		
				TSM (5.6–145.1 mg L^{-1})	Empirical: 745 nm	0.76		
				Algae bloom species	Empirical IGAG: 555, 660, 745 nm	—	Yellow Sea and East China Sea	Son, Choi, Kim, & Park, 2015
				Diurnal changes of algae bloom species	Empirical AFAI: 660, 745, 865 nm	—	Lake Taihu	Qi et al., 2018
				CDOM (2.9–65 cm^{-1})†	Quasi-analytical: 490, 555, 680 nm	0.70	Yangtze River Estuary	Wang, Shen, Sokoletsky, & Sun, 2017
				DOC (3.0–8.7 mg L^{-1})	Empirical: 490, 660 nm	0.73	Lake Taihu	Huang, Li, et al., 2017
				SPM (0.25–0.7 g L^{-1})	Semi-analytical: 555, 660, 865 nm	0.81	Yangtze River Estuary	Pan, Shen, & Wei, 2018
				TSM (10–5000 mg L^{-1})	Empirical SAI: 490, 555,745 nm	0.88	Hangzhou Bay	Liu, Liu, Li, et al., 2018
				Z_{SD}(0.5–14 m)	Semi-analytical: 490, 683 nm	0.90	Yellow-Bohai Sea	Mao, Wang, Qiu, Sun, & Bilal, 2018
MODIS	Aqua (USA)	2330	250/500/1000	CDOM (12–113 cm^{-1})‡	Empirical: 412, 443, 667, 784 nm	0.71	Pearl River Estuary	Liu, Bai, et al., 2018
				POC (0.3–35 mg L^{-1})	Empirical: 645, 859 nm	0.73	Lake Taihu	Huang, Jiang, et al., 2017
				POC (190–459 mg m^{-3})	Empirical: 443, 555 nm	0.72	Yellow-Bohai Sea	Fan, Wang, Zhang, & Yu, 2018
				POC(17.6–687.5 mg m^{-3})	Empirical: 443, 555 nm	0.94	South China Sea	Hu et al., 2016
				SPM (0–80 mg L^{-1})	Empirical: 645, 1240 nm	0.64	Lake Hongze	Cao, Duan, Shen, et al., 2018
				SSC (3–55 mg L^{-1})	Empirical: 555, 645 nm	0.81	Pearl River Estuary	Zhan, Wu, Wei, Tang, & Zhan, 2019
MODIS	Terra (USA)	2330	250/500/1000	Chla (0.07–1.74 mg m^{-3})	Empirical FLH: 667, 678, 748 nm	0.88	Northern South China Sea	Zhao & Cao, 2012
				Sloating algae area	Empirical FAI: 645, 859, 1240 nm	—	Lake Chaohu	Zhang, Ma, et al., 2015
				SPM (0–173 mg L^{-1})	Empirical: 645, 865 nm	0.76	Lake Poyang	Wu et al., 2013
				SPM (1.3–42.3 mg L^{-1})	Empirical: 645, 1242 nm	0.81	Lake Dongting	Wu, Liu, Chen, & Fei, 2014
				SSC (60–875 mg L^{-1})	Empirical: 865, 1242 nm	0.78	Yangtze River	Wang & Lu, 2010
OLCI	Sentinel 3A (Europe)	1270	300/1200	POC	Two-step classification based: 681, 779, 1020 (681, 761, 779) nm	0.63 (0.87)	Lake Taihu, Chaohu, Dianchi, Dongting, Hongze, Hengshui, and Jiajiang River	Lin et al., 2018
VIIRS	Suomi NPP (USA)	3000	375/750	Floating algae area	Empirical FAI: 645, 859, 1240 nm	—	Lake Taihu	Lyu, Wang, Jin, Li, et al., 2017
				SPM (0–80 mg L^{-1})	Empirical: 671, 1238 nm	0.72	Lake Hongze	Cao, Duan, Shen, et al., 2018
				TSM (8–103 mg L^{-1})	Semi-analytical: 745 nm	0.74	Lake Taihu	Shi et al., 2018
					Semi-analytical: 862 nm	0.76		

Note: †CDOM represented by its absorption coefficient at 443 nm; ‡CDOM represented by its absorption coefficient at 400 nm.

Table 3. Non-ocean color sensors used to remotely assess and monitor inland and coastal water qualities in China.

Sensor	Platform	Swath (km)	Spatial resolution (m)	Water quality index (range)	Algorithm and band(s) used	Performance (R^2)	Study area	Reference
TM, ETM+, OLI	Landsat (USA)	185	30	Chla (0.21–121 μg L^{-1})	Empirical: 482, 562, 655 nm	0.60	Haihe River	Guo, Wu, et al., 2016
					ANN: visible to NIR	0.94		
				Chla (0.41–31μg L^{-1})	Empirical: 482, 562, 655 nm	0.80	Xin'anjiang reservoir	Li et al., 2018
				Chla (0.3–13 μg L^{-1})	Empirical: 443, 655 nm	0.79	Hong Kong coastal waters	Nazeer & Nichol, 2016a
				floating algae area	Empirical AFAI: Green, Red NIR, SWIR bands	—	Lake Hulun	Fang et al., 2019
				floating algae area	Empirical FAH: Green, Red NIR bands	—	Yellow Sea and East China Sea	Xing & Hu, 2016
				phycocyanin PC (80–700 mg m^{-3})	Empirical: Blue, Green, Red, and NIR bands	0.56–0.85	Lake Dianchi	Sun et al., 2015
				SSC (22–2610 g m^{-3})	Empirical: 835 nm	0.88	Yangtze River	Wang et al., 2009
				SSC (0–2800 mg L^{-1})	Empirical: NIR band	0.87	Mekong River	Suif, Fleifle, Yoshimura, & Saavedra, 2016
				SSC (1–4000 mg L^{-1})	Empirical: red band	0.80	Yellow River Estuary	Zhang, Yao, et al., 2014
				SSC (203–750 mg L^{-1})	Empirical: NIR band	0.98	Hangzhou Bay	Cai, Tang, & Li, 2015
				SSC (4.3–104 mg L^{-1})	Empirical: 840 nm	0.84	Bohai sea	Kong et al., 2015
					Empirical: 560, 660 nm	0.98		
				SPM (6.97–74.5 g m^{-3})	Empirical: 560, 655 nm	0.98	Yellow River Estuary	Qiu et al., 2017
				SPM (0.25–0.7 g L^{-1})	Semi-analytical: 561, 655, 865 nm		Yangtze River Estuary	Pan et al., 2018
				TSM (∼0.0–140 g m^{-3})	Empirical: 655 nm	0.79	Pearl River Estuary	Gao et al., 2019
				TSS (4.3–577 mg L^{-1})	Empirical: Red, NIR bands	0.72	Pearl River Estuary, Yangtze River Estuary	Wang, Chen, et al., 2017
				Turbidity (15.8–130 NTU)	Empirical: 440, 480, 560 nm	0.92	Hanjiang River	Shen & Feng, 2018
				Z_{SD} (0.1–1.05 m)	Empirical: 560, 655 nm	0.81	Three Gorges Reservoir and Lake Dongting	Ren et al., 2018
				Z_{SD} (0.25–1.15 m)	Empirical: Blue, NIR bands	0.86	Lake Liangzi	Xu, Huang, Zhang, & Yu, 2018
CCD	HJ-1A/B (China)	360	30	Floating algae area	Empirical: 4 bands 430–900 nm	—	Lake Gaoyang and Hanfeng	Zhou et al., 2017
				Floating algae area	Empirical FAH: 540, 660, 830 nm	—	Yellow Sea and East China Sea	Xing & Hu, 2016
				TP (0.04–1.89mg L^{-1})	Empirical: 660, 830 nm	0.95	Lake Chaohu	Gao et al., 2015
				TIN (0.15–0.5mg L^{-1})	Empirical random forest: 4 bands 430–900 nm	0.40	Pearl River Estuary	Liu, Liu, Li, Ding, & Jiang, 2014
				TSS (9.89–36 mg L^{-1})	Empirical: 540, 660 nm	0.81	Deep Bay	Tian, Wai, et al., 2014
HSI	HJ-1A/B (China)	50	100	Chla(1.8–40 mg m^{-3})	Red-NIR: 634, 711, 754 nm	0.77	Xiamen coastal area	Tian, Cao, et al., 2014
WFV	GF-1 (China)	800	16	TSM (15–65 mg L^{-1})	Empirical: 560, 660 nm	0.62	Deep Bay	Tian et al., 2016
Hyperion	EO-1 (USA)	7.7	30	Chla (4.8–93 mg m^{-3})	Empirical: 684, 690, 718 nm	0.95	Pearl River Estuary	Chen, Fang, Li, Chen, & Huang, 2011
				TSM (8.4–46 mg L^{-1})	Empirical:813, 559 nm	0.71	Pearl River Estuary	Liu, Fu, Xu, & Shen, 2012
				TSM (6–140 mg L^{-1})	Empirical:600, 610 nm	0.68	Pearl River Estuary	Xing, Lou, Chen, & Shi, 2013
				TSS (7.0–241 mg L^{-1})	Empirical: 527, 680 nm	0.94	Pearl River Estuary	Fang, Chen, Li, & Li, 2009
WV-2	Spacecraft (USA)	16.4	1.8	Chla (1–8 μg L^{-1})	Empirical:545, 725nm	0.84	Guanting Reservoir	Wang, Gong, et al., 2018
MSI	Sentinel-2 (European Union)	290	10/20	CDOM (1.7–3.3 m^{-1})	Empirical: 783, 842 nm	0.51	Lake Poyang	Xu, Fang, et al., 2018
AISA	Airborne			Pigment: Chla (0.41–4.21)	Empirical: 550, 560 nm	0.71	Lake Chaohu and Dianchi	Shi, Zhang, et al., 2015

Note: CDOM represented by its absorption coefficient at 355 nm.

thirteen sensors from 1996 to 2011, such as SeaWiFS (USA, 1997) and MERIS (Europe, 2002), and eight polar-orbiting sensors from 1996 to 2017, such as MODIS (USA, 1999) and OLCI (Europe, 2016) (IOCCG, 2012).

Chla estimates are mainly based on semi-analytical models using two kinds of R_{rs} values from the abovementioned ocean color sensors, i.e. the green/blue ratio using two to four bands (abbreviated as the OC algorithm) and the red-NIR ratio using two or three bands (abbreviated as red-NIR algorithm). The red-NIR algorithm exhibits limited bias at high Chla, i.e. 10–100 mg m^{-3} (Odermatt et al., 2012). With the aid of field hyperspectral measurements in Lake Taihu (Chla varying from 1 to 89 mg m^{-3}), Le et al. (2009) found that the Chla estimation from a three-band red-NIR algorithm generally performed better than those from a two-band red-NIR algorithm and a proposed four-band algorithm performed much better than a three-band algorithm. To broaden the applicability of the red-NIR algorithm in complex turbid water, Yang, Matsushita, Chen, and Fukushima (2011) proposed a semi-analytical model-optimizing and look-up-table method. The results from using this method in Lake Dianchi indicated that the MERIS-based Chla estimates were accurate. To address a single model that may not be suitable for optically complex waterbodies, classification-based methods were proposed, and waterbodies were classified based on their optical properties. Then, Chla in the classified waterbodies were estimated using the given method (Le et al., 2011). The application of such classification-based methods with MERIS and MODIS datasets in turbid Lake Taihu, the East China Sea, Yellow Sea, and Bohai Sea exhibited effective performance (Shanmugam, He, Singh, & Varunan, 2018; Zhang et al., 2019).

In addition to improving the red-NIR algorithm, Song et al. (2013) developed an adaptive method based on genetic algorithms (GA-PLS) and field spectral datasets. This method was validated in several lakes, including Lake Taihu, which indicated that GA-PLS outperformed the three-band red-NIR algorithm for Chla estimates. Recently, to address the low efficiency of GA-PLS, Cao, Ye, et al. (2018) modified and applied a population-based evolutionary algorithm (MDBPSO) in the eutrophic Lake Weishan based on HJ-1A HSI imagery and found that MDBPSO could precisely estimate Chla and performed better than GA-PLS. Several studies tested the combination of active polarimetric synthetic aperture radar (SAR) data with hyperspectral data to improve Chla estimations for turbid inland waters, such as in Lake Taihu (Zhang, Martti, et al., 2018), while others proposed the application of machine learning methods to improve the quantity and quality of MODIS Chla data (Chen et al., 2019).

The relatively coarse resolution of ocean color data (~1000 m) cannot capture small inland rivers and waterbodies or identify their heterogeneity.

Thus, data from other high-spatial-resolution non-ocean-color sensors, such as WV-2 (~2 m) (Wang, Gong, & Pu, 2018) and Landsat (~ 30 m) (Guo, Wu, et al., 2016), are commonly used to retrieve water quality indices, including Chla (Table 3). However, the estimates are commonly based on empirical methods due to the low spectral resolution of these sensors (i.e. normally 4 bands in visible light). Several studies have developed data fusion methods to enhance the spatial resolution of ocean-color-based Chla estimates using high-spatial-resolution images (e.g. CCD or OLI) (Guo, Li, et al., 2016; Fu, Xu, Zhang, & Sun, 2018).

3.2.2. CDOM

CDOM is commonly estimated from empirical methods using single bands, band ratios, or band arithmetic (Odermatt et al., 2012 and references therein). Band ratios, such as R_{rs} in the blue (~400–500 nm)/R_{rs} in the green or red (~500–700 nm), are generally correlated well with CDOM (Matthews, 2011). However, suitable sensors to detect CDOM are limited because significant absorption by CDOM is restricted to the blue wavelengths, and absorption of CDOM and Chla coincide in the blue region, leading to difficulty in separating the signals (Odermatt et al., 2012 and references therein). These factors explain why CDOM retrieval studies are less common than those estimating Chla and SPM in China (Tables 1 to 3).

3.2.3. SPM

SPM is the total mass of suspended matter (also called TSM), including suspended solids (SS) such as suspended sediment. Similar to CDOM, SPM (TSM) and the related SS and suspended sediment concentration (SSC) are often estimated using empirical methods and red to NIR band(s) (Odermatt et al., 2012 and references therein). For example, Wang, Lu, Liew, and Zhou (2009) successfully estimated SSC with large variation (22–2610 g m^{-3}) in the Yangtze River using regression analysis and Landsat ETM + band 4 (860 nm). Later, they developed an empirical algorithm between SSC and band 2 (865 nm) minus band 5 (1240 nm) of MODIS to obtain estimates for the Yangtze River with high temporal resolution (Wang & Lu, 2010). Feng, Hu, Chen, and Song (2014) established a piecewise TSM algorithm using MODIS R_{rs} data at 645 and 859 nm over the turbid Yangtze River Estuary and found that the TSM decreased significantly due to the impoundment of the Three Gorges Dam. To address the limitations of the empirical methods, TSM was estimated using a semi-analytical method based on the intrinsic relationship between TSM and its backscattering characteristics. Shi, Zhang, and Wang (2018) demonstrated that TSM could be accurately estimated using the backscattering coefficients derived from the VIIRS NIR band in turbid Lake Taihu.

3.2.4. Other indices

In addition to the achievements mentioned above, several water quality indices required for management in China have been proposed. To further distinguish harmful cyanobacteria in inland lakes due to Chla limitations (i.e. different phytoplankton species could not be identified), Qi, Hu, Duan, Cannizzaro, and Ma (2014) proposed a novel algorithm using MERIS R_{rs} at 620 nm to derive cyanobacterial phycocyanin pigment concentrations (PC) for inland lakes (i.e. Lake Taihu and Dianchi). This algorithm exhibited good performance for PC varying from 1–300 mg m^{-3} under nearly all observing conditions except thick clouds. Later, Sun, Hu, Qiu, and Shi (2015) developed a new PC retrieval algorithm for Lake Dianchi based on visible-NIR Landsat bands. Recently, Ling et al. (2018) proposed a new method based on fluorescence emission signals at 550 and 700 nm obtained from the HOBI Labs Hydroscat-6P to identify phytoplankton community structures in the Bohai Sea, Yellow Sea, and East China Sea, and the method was feasible for identifying dominant algae species. RS of BOD, COD, DO, dissolved inorganic nitrogen (DIN), ammonia nitrogen, and nitrate nitrogen using empirical methods has been only reported in a limited number of studies (Wang & Ma, 2001; Wang, Xia, Fu, & Sheng, 2004; He, Chen, Liu, & Chen, 2008; Yu et al., 2016).

3.3. Advances in sensor design and corresponding algorithm development

Although spectral bands at 480–580 nm designed for ocean color RS have been onboard the Chinese FY series meteorological satellites since 1988, the first specific ocean color sensor launched in China was the Chinese moderate imaging spectra radiometer (CMODIS). This sensor has 34 bands covering 403 nm to 12.5 μm and is onboard the SZ-3 spacecraft launched in March 2002 (Chen, Shao, Guo, Wang, & Zhu, 2003). However, the first ocean color satellite was HY-1A, which was launched in the same year and carried the Chinese Ocean Color and Temperature Scanner (COCTS), with 10 bands covering 402 nm to 12.5 μm (Figure 6). As a pilot sensor, certain experiences have been accumulated and applied to subsequent ocean color missions, i.e. COCTS is currently in orbit onboard HY-1B, which was launched in 2007. In 2016, China launched its next-generation ocean experimental sensor, Moderate-Resolution Wide-Wavelengths Imager (MWI) with 14 visible-NIR bands (400–1040 nm), 2 SWIR bands (1243–1252 nm and 1630–1654 nm), and 2 thermal infrared (TIR) bands

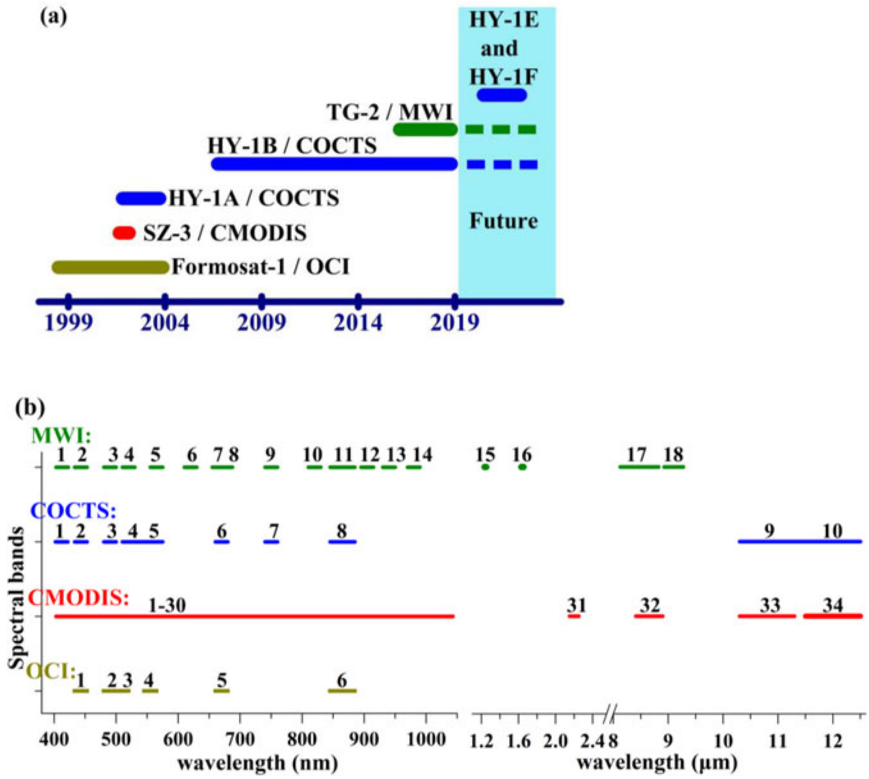

Figure 6. Timeline of Chinese ocean color sensors (a) and spectral information (b). Note: Formosat-1, formerly known as ROCSAT-1, was designed in Taiwan, and the other sensors were designed and launched in mainland China; the numbers in b represent the band order.

(8.125–8.825 μm and 8.925–9.275 μm) (Figure 6), which is onboard the TG-2 Space Lab.

Prior to the launch of MWI, studies written in English about these sensors were mainly focused on processing methods, such as data quality improvements (Chen et al., 2003), atmospheric correction (He, Pan, & Zhu, 2005), and cross-calibration to obtain radiances (Pan, He, & Mao, 2003; Pan, He, & Zhu, 2004; Liu, Merchant, Guan, & Mittaz, 2018). A limited number of studies have been performed on water quality. Of these studies, one retrieved water-leaving radiance (Pan et al., 2004), one studied the establishment of algorithms for CMODIS-based Chla determinations (Mao, Zhu, & Gong, 2007), and another retrieved SSC in the Yangtze River Estuary using CMODIS (Han, Jin, & Yun, 2006). In contrast, more attention has been paid to MWI than the other sensors. He et al. (2017) presented preliminary but relatively detailed retrieval methods and products (i.e. L_w, Chla, and TSM) from MWI, and the validation results indicated that the products were of good quality when compared to that of in situ measurements as well as other datasets, such as GOCI, MODIS/Aqua and VIIRS, in the turbid Yangtze River Estuary. Cao, Duan, Song, et al. (2018)

assessed the MWI-retrieved inland water estimates (i.e. R_{rs}, algal blooms, and TSM) and found that the overall performance was comparable to that of current ocean color sensors. However, Zhou, Tian, Li, Song, and Li (2018) suggested that a cross-calibration of MWI using MODIS data could benefit the accuracy of water quality index retrievals in both the open ocean and inland Lake Taihu.

3.4. Advances in RS-based operational systems and their applications

To monitor the environment and resources nationwide, including the water environment, the SEC, which is an MEP department in China, established an operational satellite application system for water quality monitoring. Initially, the operation of the system was mainly based on the Terra/Aqua-MODIS and Chinese HJ-1 satellites. Several years ago, with the development and application of Chinese high-resolution satellites, the SEC constructed a new high-resolution RS operational application system for water environmental monitoring that mainly depends on the Chinese GF satellite series (from GF-1 to GF-7) and other satellites with similar resolutions. These two operational systems can generate continual products retrieved from the same data series (e.g. Figure 7) and provide crucial information on algae blooms, water color, black and odorous waterbodies, drinking water source risks, rural nonpoint source pollution, red tides, oil spills, and thermal water pollution and thermal discharge from nuclear plants. These systems have improved the monitoring ability and played a great role in the state of water environmental monitoring (Zhao et al., 2017). For example, the recent SANCHI oil tanker collision accident on January 6, 2018, in the East China Sea caused an intense fire that continued for one week, resulting in serious ecosystem damage. The system collected the available satellite images, including GF-3 and GF-4, over the area beginning on January 8, which provided critical information for decision makers. However, obvious shortcomings need to be resolved to increase the ability of water quality monitoring. Specifically, the current system products are mainly qualitative and provide limited quantitative information on water indices. Additionally, validations of the products are scarce due to limited observational sites. Furthermore, fine-resolution satellites (i.e. $\sim$1 m) with short revisit times (i.e. one to two days) are lacking.

3.5. Advances in monitoring sudden water pollution accidents

This section focuses on oil spills (red tides) in the Chinese coastal and sea regions because sea oil spill accidents (red tides) are increasing. Oil spills are driven by the exploitation and transportation of marine oil (Xiong, Long, Tang, Wan, & Li, 2015), whereas red tide blooms (also termed

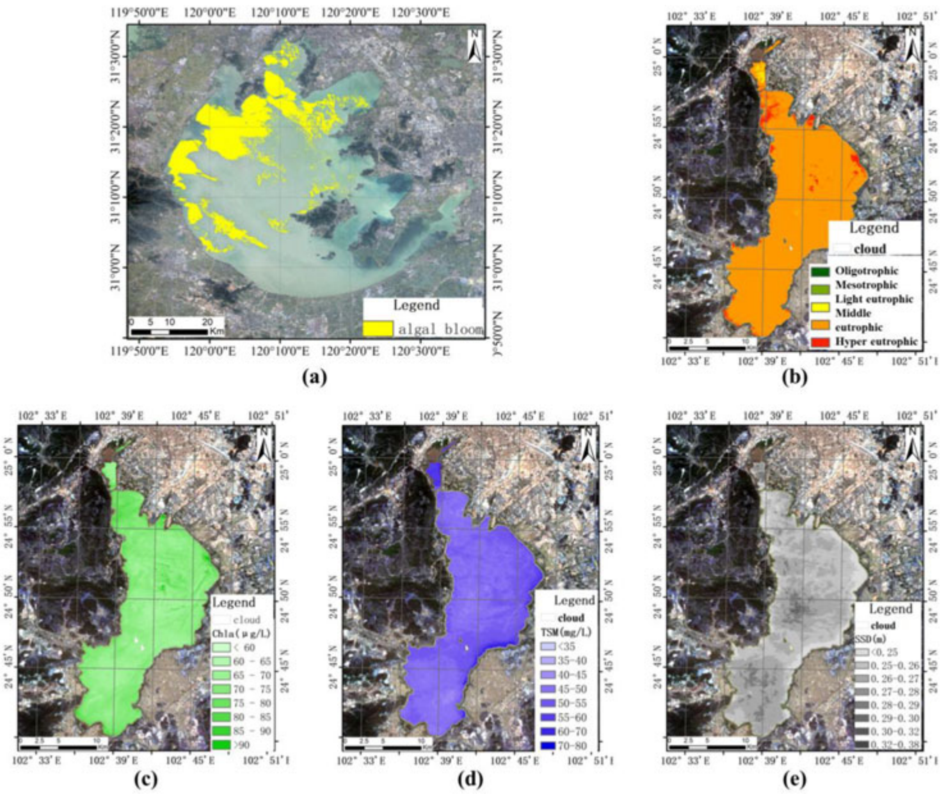

Figure 7. Examples showing the water quality products generated by the operational satellite system operated by the Satellite Environment Center, the Ministry of Ecology and Environment of China: (a) algal bloom in Lake Taihu based on GF1-WFV October 27, 2018; (b) to (e) are the level of eutrophication, chlorophyll-a concentration, suspended solids, and transparency of Lake Dianchi, respectively, based on GF1-WFV April 11, 2017. Note: GF1 images are RBG = 432.

harmful algal blooms, HABs) are driven by rising temperatures and pollution (Zhao, Zhao, Zhang, & Zhang, 2004; Lu et al., 2018).

In addition to the Chinese government, scientists have also been involved in studies related to detecting and monitoring oil spills. Xu et al. (2013) used remotely sensed oil spill areas as an important model input for simulating oil spill trajectories and found that the method performed well in the semi-enclosed shallow Bohai Sea. Liu, Li, Liu, Xie, and Muller (2018) investigated the reflectance features of oil-polluted sea ice and suggested that AVIRIS, MODIS, Sentinel3-OLCI, Landsat8-OLI, and GF-2 could be adopted to detect oil spills on sea ice. Jin et al. (2018) proposed a method to identify oil slicks under various levels of sunglint in high-resolution images (5 m) from the airborne imaging spectrometer for applications (AISA). Sun, Lu, Liu, Wang, and Hu (2018) further showed that a combination of numerical models and available RS datasets could improve the monitoring ability and be of assistance when oil spills occur. In addition, several monitoring systems have been developed. For example, Shi, Yu, et al. (2015) designed an airborne ultraviolet imaging system to monitor and track oil slicks in coastal regions. Yan, Wang, Chen, Zhao, and Huang (2015) developed a dynamic RS data-driven system to detect oil spills, and tests using several accidents as examples indicated that the system could improve oil spill simulations and diffusion forecasting. Gao, Li, Lin, and He (2017) designed an inelastic hyperspectral lidar system to discriminate oil pollution; laboratory experiments indicated that the system was successful and could be applied in both marine and terrestrial environments. Chiu et al. (2018) proposed an oil spill forecasting system using X-band radar, and a case study in Taipei indicated that the forecasted oil spill trajectories were comparable to field observations. Hou, Li, Liu, Liu, and Wang (2018) designed an ultraviolet-induced fluorescence and fluorescence filter system to monitor oil spills, and tests performed at the port of Lingshui (Yellow Sea, China) indicated that the system could detect oil spills at an early stage. The detection of oil spills using either active RS sensors (e.g. SAR) or passive optical RS sensors with the aid of sunglint is possible.

The remote detection of red tides is commonly based on R_{rs} (or Chla) and bio-optical properties (Ahn & Shanmugam, 2006; Shen, Xu, & Guo, 2012). Methods have been developed to monitor HABs and identify phytoplankton bloom types using ocean color sensors, such as GOCI, MODIS, and MERIS (Lou & Hu, 2014; Xu, Pan, Mao, & Tao, 2014; Tao et al., 2015, 2017). With a high temporal frequency of eight times per day, GOCI could be applied to investigate diurnal changes in cyanobacteria blooms, which may be caused by the vertical migration of cyanobacteria cells and provide guidance for future field studies (Qi, Hu, Visser, & Ma, 2018). To further improve the understanding of HABs, the phytoplankton size class (PSC) should be identified. Several recent studies have performed such identifications over the Chinese continental shelf sea based on GOCI, MERIS, MODIS, and SeaWiFS (Hu et al., 2018; Sun, Shen, et al., 2018; Sun, Wu, et al., 2018; Zhang, Wang, et al., 2018).

4. Challenges

4.1. RS-based water quality information does not meet the demands of China's war on pollution

In 2014, the Chinese Central Government declared war on pollution and subsequently amended the Water Pollution Prevention and Control Law (Peking University Center for Legal Information, 2017). Since that time, the government has issued firm policies, such as the Water Pollution Prevention and Control Action Plan (10-Point Water Plan) (The State Council, 2015), and unveiled guidelines to comprehensively enhance ecological and environmental protection (The State Council, 2018), including controlling water pollution and restoring degraded water ecosystems.

Correspondingly, detailed actions were initiated, such as urban water pollution control (Xinhua News, 2018a) and a difficult battle against pollution in the Bohai Sea area (Xinhua News, 2018b). According to the Bulletin of first National Census for Water (MWR and NBS, 2013), lakes with an area $<10\,\text{km}^2$ accounted for 77.4% of the investigated lakes, whereas the ratio of small reservoirs (total storage $<10^6\ \text{m}^3$) was 95.2%. We found that the minimum area of the studied lakes was at least $10\,\text{km}^2$ (Zhang, Yao, et al., 2014; Feng, Hou, & Zheng, 2019). In addition, more than 2000 black odorous waters with a total length of 5798 km in urban areas that needed to be restored were identified in the 13th Five-year Plan (2016–2020) (MOHURD, 2017). Particularly in relatively developed delta cities, urban rivers are often seriously polluted and require urgent remediation. As such, water pollution control and the restoration of aquatic ecosystems require adequate information. However, RS has mainly been applied in relatively large lakes and reservoirs, and major gaps still exist that prevent such information from being obtained for most inland waterbodies using RS data at the required scale (Han et al., 2016). Therefore, remotely assessing and monitoring the water quality of these waters is currently limited due to a lack of professional sensors for inland waters, although many satellite sensors provide big data. This lack of sensors has caused a mismatch between the demands of the war on pollution in Chinese inland waters and the availability of adequate information.

4.2. Lack of professional sensors for inland waters

As shown in the abovementioned context and Tables 1 to 3, the sensors used for assessing inland water quality are designed for either ocean water or land surfaces, including the Chinese Hyperspectral Imager (HSI) (115 bands covering 450–950 nm) on board HJ-1A and the Visual and Infrared Multispectral Sensor (VIMS) (330 bands covering 400–2500 nm) onboard the recent launched GF-5 satellite. While the data from these sensors provide distinct spectral characteristics of water absorption and reflectance, their coarse spatial resolution (kilometer-scale) is insufficient for studying inland waterbodies with areas smaller than $12\,\text{km}^2$, as indicated by Feng et al. (2019). However, inland rivers are typically short laterally, e.g. the width of the Yangtze River is normally $<3\,\text{km}$ (Chen, Li, Shen, & Wang, 2001); hence, coarse resolution may not capture these waters well, or the signals may contain large uncertainty. While sensors with decameter-scale pixel resolution (or better) designed for land monitoring can capture inland waters with small areas or widths, the sensors may not have spectral bands for water or the spectral resolution may not adequately capture the characteristics of water absorption and reflectance (see Section 4.3 for details).

For example, most sensors have only four bands in the visible spectrum. With limited spectral bands, water quality indices are commonly retrieved from empirical methods (examples in Table 3) that may have local applications. Even HIS and VIMS provide data with high spectral resolution at 30 m, the narrow swath (~60 km) is far insufficient for water environment monitoring at the national scale. The lack of professional sensors for inland waters that can meet the demands required to tackle the water pollution crisis nationwide is a major challenge for water resource monitoring and management in China.

4.3. Dilemma between spatial, spectral, and temporal resolution

High spatial resolution is necessary to capture and provide accurate information for inland rivers and small lakes and reservoirs. However, a sensor with high spatial resolution should have a small instantaneous field of view (IFOV). A small IFOV reduces detectable energy because as the IFOV decreases, radiometric resolution decreases, and fine energy differences cannot be detected. Thus, to maintain the radiometric resolution without decreasing the spatial resolution, the detected wavelength range should be broadened for a given band, which unfortunately reduces the spectral resolution of the sensor. Conversely, a relatively coarse spatial resolution would improve the radiometric and/or spectral resolution. The balance between these three types of resolution is a major challenge in sensor design (Figures 8 and 9). In addition, high-spatial-resolution data with low spectral

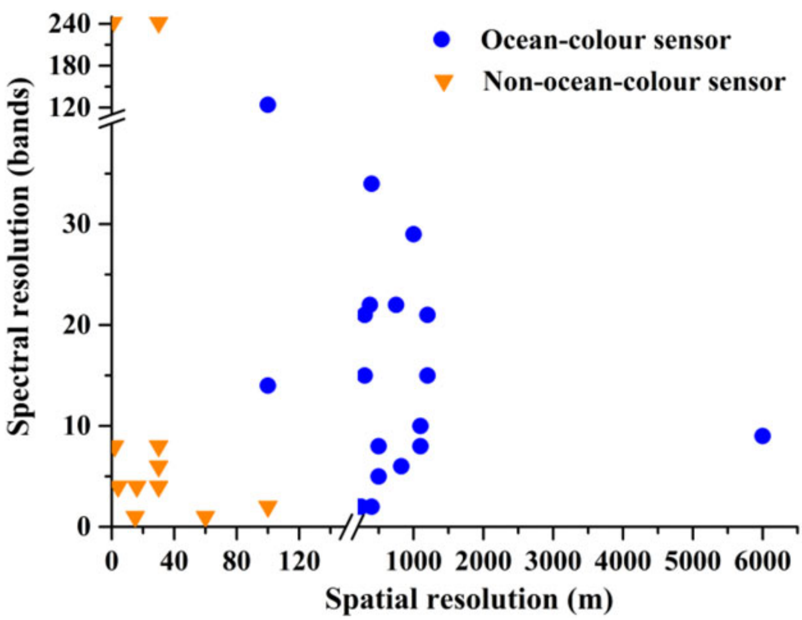

Figure 8. The spatial and spectral resolutions of the sensors listed in Tables 1 to 3.

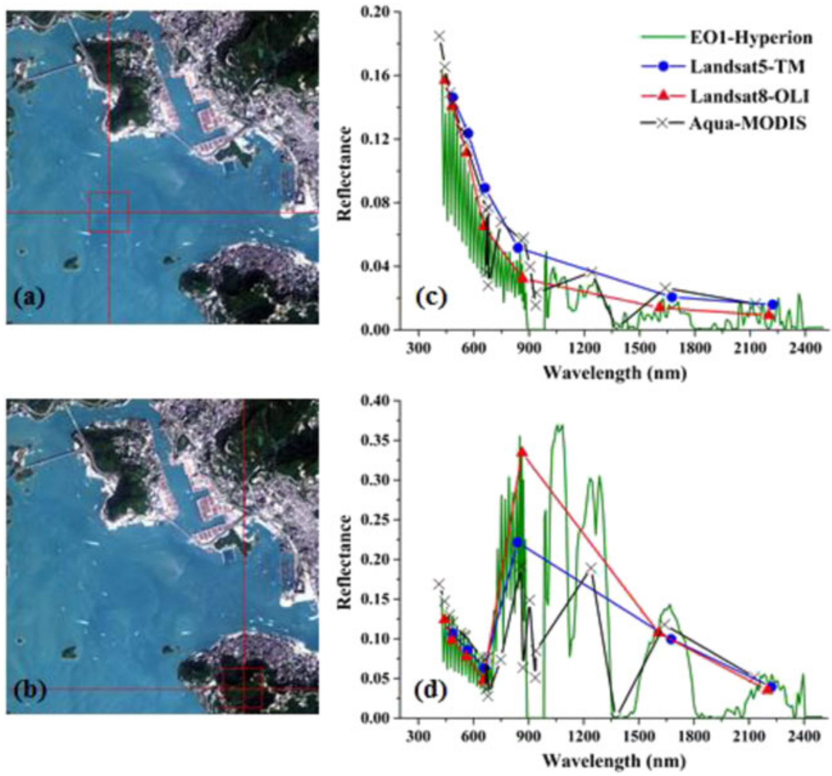

Figure 9. An example showing the impact of spectral bands of a sensor on the ability to detect fine differences: false color images are in the left column, and red crosses are the target water (a) and vegetation (b) pixels; the corresponding spectral characteristics for the water (c) and vegetation (d) pixels are in the right column. Note: the false-color image that was combined using a Landsat 8 (RBG = 432, path 122 and row 44) scanned on October 23, 2017, covers the coastal region of Hong Kong; the acquisition dates of the sensors differ.

resolution commonly have a low signal-to-noise ratio (SNR), such as Landsat-8 OLI, as summarized in Zheng and DiGiacomo (2017). Because the SNR would affect the ability to distinguish target information from the surrounding water, a high SNR must be preferred. Furthermore, water quality monitoring requires high temporal resolution. Except for GOCI (eight times per day) and MODIS (twice per day), other satellite sensors normally provide data in a several-day cycle, which also hampers timely water quality monitoring.

5. Future outlooks

Information on inland water quality is essential for water resource management and aquatic ecosystem restoration. To address the problems discussed above, especially for the large number of unstudied small lakes and reservoirs, a possible solution may be to assess the water quality of these inland waters first using empirical methods and current high-resolution sensors, such as the GF series. Inland waters can be classified into certain categories based on primary water quality information, and typical waters in each class can be selected to perform further studies, including the establishment of field monitoring networks, measurement of water optical properties and the development of water quality retrieval algorithms. Additionally, these processes can also result in the accumulation of fundamental experience for developing inland water sensors.

Moreover, the long-term fundamental solution is to accelerate the development and launch of inland water sensors. Even the current MWI has a relatively poor ability to retrieve Chla in inland lakes due to design limitations, i.e. a failure to detect signals at 700–710 nm (Cao, Duan, Song, et al., 2018). Such limitations should be considered in the design of new sensors. In addition, these new sensors should be designed with designing high spatial and spectral resolution, a wide dynamic swath, a high SNR, and high revisit capability, e.g. the sensors on HJ-2 to be launched in 2020. Achieving such a goal may require a substantial amount of time and funding. Therefore, unmanned aerial vehicles (UAVs), which have been proven to be useful for assessing and monitoring water quality (Shang et al., 2017; Xu, Gao, et al., 2018), can be used as an alternative to monitor inland waters.

Considering the water pollution conditions and rapid urbanization in China, monitoring urban black odorous waters is a matter of great urgency that is good not only for the war on water pollution but also for building eco-cities and livable civic environments. In addition, future water resource management may require switching from single water index monitoring to aquatic ecosystem monitoring, which requires even more information and generates more challenges for RS monitoring.

Furthermore, some of the major international rivers in Asia originate in China; therefore, China faces complex cross-border water and related ecological problems. Especially under the Chinese government's Belt and Road Initiative development strategy, utilizing and protecting these international rivers can influence China's regional cooperation strategies with related countries; therefore, the collection of detailed information on these remote international rivers by RS is urgently required.

Finally, the quality consistency of RS data should be considered when estimating water quality (Pahlevan, Chittimalli, Balasubramanian, & Vellucci, 2019) not only for different sensor types but also for similar sensor series and even the same sensor. Signal attenuation occurs over time for a given sensor and lowers the quality of scanned data. Studies on the impact of such inconsistencies in data quality on RS estimates are limited in China, and few studies have been published, e.g. by Liu's group (Fan & Liu, 2014, 2016, 2017).

6. Summary

Water quality information across a wide spatiotemporal scale is crucial for water pollution control and aquatic ecosystem restoration in China, and these data can be obtained at such scales by only RS methods. Recent achievements in remotely assessing and monitoring coastal and inland water quality in China were reviewed in this paper. Particular focus was placed on the progress of sensor design and algorithm development as well as on the necessary methods for processing RS data prior to water quality retrieval. Additionally, advances in monitoring sudden water pollution accidents such as oil spills and HABs were discussed.

Major challenges for future studies were identified in this paper, including 1) a large gap (or mismatch) between the water quality information requirements and current RS datasets due to a lack of professional inland water sensors with proper spatiotemporal resolution, 2) a scarcity of monitoring planning (or network) for inland waters and field experiments for studying the optical properties of these waterbodies, and 3) the fact that the priority of RS should be urban black odorous waters and international rivers. This review may help enhance the understanding of remote sensing-based water quality in China. Additionally, this review will hopefully provide scientific guidelines for obtaining information about coastal and inland waters and assist water resource managers and aquatic ecologists in controlling water pollution.

Acknowledgments

We gratefully acknowledge the financial support from the National Key R&D Program of China (2017YFB0503905), the Major Projects of High Resolution Earth Observation Systems of National Science and Technology (05-Y30B01-9001-19/20-1), and the National Natural Science Foundation of China (41671416). We also thank the USGS for providing Landsat, MODIS, and EO datasets. We are grateful to the editors and reviewers for their insightful and constructive comments.

Disclosure statement

No potential conflict of interest was reported by the authors.

References

Ahn, Y. H., & Shanmugam, P. (2006). Detecting the red tide algal blooms from satellite ocean colorobservations in optically-complex Northeast-Asia Coastal waters. *Remote Sensing of Environment*, *103*(4), 419–437. doi:10.1016/j.rse.2006.04.007

Behrenfeld, M. J., Boss, E., Siegel, D. A., & Shea, D. M. (2005). Carbon based ocean productivity and phytoplankton physiology from space. *Global Biogeochemical Cycles*, *19*(1), 1–14. doi:10.1029/2004GB002299

Cai, B., Zhang, W., Hubacek, K., Feng, K., Li, Z., Liu, Y., & Liu, Y. (2019). Drivers of virtual water flows on regional water scarcity in China. *Journal of Cleaner Production*, *207*, 1112–1122. doi:10.1016/j.jclepro.2018.10.077

Cai, L. N., Tang, D. L., & Li, C. Y. (2015). An investigation of spatial variation of suspended sediment concentration induced by a bay bridge based on Landsat TM and OLI data. *Advances in Space Research*, *56*(2), 293–303. doi:10.1016/j.asr.2015.04.015

Cao, Y., Ye, Y. T., Zhao, H. L., Jiang, Y. Z., Wang, H., Shang, Y. Z., & Wang, J. F. (2018). Remote sensing of water quality based on HJ-1A HSI imagery with modified discrete binary particle swarm optimization-partial least squares (MDBPSO-PLS) in inland waters: A case in Weishan Lake. *Ecological Informatics*, *44*(5), 21–32. doi:10.1016/j.ecoinf.2018.01.004

Cao, Z., Duan, H., Shen, M., Ma, R., Xue, K., Liu, D., & Xiao, Q. (2018). Using VIIRS/NPP and MODIS/aqua data to provide a continuous record of suspended particulate matter in a highly turbid inland lake. *International Journal of Applied Earth Observation and Geoinformation*, *64*, 256–265. doi:10.1016/j.jag.2017.09.012

Cao, Z., Duan, H., Song, Q., Shen, M., Ma, R., & Liu, D. (2018). Evaluation of the sensitivity of China's next-generation ocean satellite sensor MWI onboard the tiangong-2 space lab over inland waters. *International Journal of Applied Earth Observation and Geoinformation*, *71*, 109–120. doi:10.1016/j.jag.2018.05.012

Carpenter, D. J., & Carpenter, S. M. (1983). Modeling inland water quality using Landsat data. *Remote Sensing of Environment*, *13*(4), 345–352. doi:10.1016/0034-4257(83)90035-4

Chang, N. B., Imen, S., & Vannah, B. (2015). Remote sensing for monitoring surface water quality status and ecosystem state in relation to the nutrient cycle: A 40-year perspective. *Critical Reviews in Environmental Science and Technology*, *45*(2), 101–166. doi:10.1080/10643389.2013.829981

Chapra, S. C., Boehlert, B., Fant, C. W., Bierman, V. J., Henderson, J., Mills, D., … Martinich, J. (2017). Climate change impacts on harmful algal blooms in U.S. freshwater: A screening-level assessment. *Environmental Science & Technology*, *51*(16), 8933–8943. doi:10.1021/acs.est.7b01498

Chen, J., Shao, Y., Guo, H., Wang, W., & Zhu, B. (2003). Destriping CMODIS data by power filtering. *IEEE Transactions on Geoscience and Remote Sensing*, *41*, 2119–2124.

Chen, S. L., Hu, C., Barnes, B. B., Xie, Y. Y., Lin, G., & Qiu, Z. F. (2019). Improving ocean color data coverage through machine learning. *Remote Sensing of Environment*, *222*(3), 286–302. doi:10.1016/j.rse.2018.12.023

Chen, S. S., Fang, L. G., Li, H. L., Chen, W. Q., & Huang, W. (2011). R. Evaluation of a three-band model for estimating chlorophyll-a concentration in tidal reaches of the Pearl River Estuary, China. *ISPRS Journal of Photogrammetry and Remote Sensing*, *66*(3), 356–364. doi:10.1016/j.isprsjprs.2011.01.004

Chen, Z., Li, J., Shen, H., & Wang, Z. (2001). Yangtze River of China: Historical analysis of discharge variability and sediment flux. *Geomorphology*, *41*(2–3), 77–91. doi:10.1016/S0169-555X(01)00106-4

Chinese Academy of Engineering (CAE). (2000). Strategic research on sustainable development of water resource in China. *Engineering Science*, *2*(8), 1–17.

Chiu, C. M., Huang, C. J., Wu, L. C., Zhang, Y. L., Chuang, Z. H., Fan, Y. M., & Yu, H. C. (2018). Forecasting of oil-spill trajectories by using SCHISM and X-band radar. *Marine Pollution Bulletin*, *137*(12), 566–581. doi:10.1016/j.marpolbul.2018.10.060

Deng, J., Zhang, Y., Qin, B., Yao, X., & Deng, Y. (2017). Trends of publications related to climate change and lake research from 1991 to 2015. *Journal of Limnology*, *76*(3), 439–450. doi:10.4081/jlimnol.2017.1612

Deng, J. M., Paerl, H. W., Qin, B., Zhang, Y., Zhu, G., Jeppesen, E., … Xu, H. (2018). Climatically-modulated decline in wind speed may strongly affect eutrophication in shallow lakes. *Science of the Total Environment*, *645*, 1361–1370. doi:10.1016/j.scitotenv.2018.07.208

Dörnhöfer, K., & Oppelt, N. (2016). Remote sensing for lake research and monitoring-recent advances. *Ecological Indicators*, *64*, 105–122. doi:10.1016/j.ecolind.2015.12.009

Du, C. G., Li, Y. M., Wang, Q., Liu, G., Zheng, Z. B., Mu, M., & Li, Y. (2017). Tempo-spatial dynamics of water quality and its response to river flow in estuary of Taihu Lake based on GOCI imagery. *Environmental Science and Pollution Research*, *24*(36), 28079–28101. doi:10.1007/s11356-017-0305-7

Fan, H., Wang, X. J., Zhang, H. B., & Yu, Z. T. (2018). Spatial and temporal variations of particulate organic carbon in the Yellow-Bohai Sea over 2002–2016. *Scientific Reports*, *8*(1), 7971. doi:10.1038/s41598-018-26373-w

Fan, X., & Liu, Y. (2014). Quantifying the relationship between intersensor images in solar reflective bands: Implications for intercalibration. *IEEE Transactions on Geoscience and Remote Sensing*, *52*, 7727–7737.

Fan, X., & Liu, Y. (2016). A global study of NDVI difference among moderate-resolution satellite sensors. *ISPRS Journal of Photogrammetry and Remote Sensing*, *121*, 177–191. doi:10.1016/j.isprsjprs.2016.09.008

Fan, X., & Liu, Y. (2017). A Generalized model for intersensor NDVI calibration and its comparison with regression approaches. *IEEE Transactions on Geoscience and Remote Sensing*, *55*(3), 1842–1852. doi:10.1109/TGRS.2016.2635802

Fang, C., Song, K. S., Shang, Y. X., Ma, J. H., Wen, Z. D., & Du, J. (2019). Remote sensing of harmful algal blooms variability for Lake Hulun using adjusted FAI (AFAI) algorithm. *Journal of Environmental Informatics*. doi:10.3808/jei.201700385

Fang, L. G., Chen, S. S., Li, D., & Li, H. L. (2009). Use of reflectance ratios as a proxy for coastal water constituent monitoring in the Pearl River Estuary. *Sensors (Basel, Switzerland)*, *9*(1), 656–673. doi:10.3390/s90100656

FAO. (2019). AQUASTAT database, Food and Agriculture Organization of the United Nations (FAO). Retrieved from http://www.fao.org/nr/water/aquastat/data/query/index.html?lang=en

Feng, L., Hou, X., Li, J., & Zheng, Y. (2018). Exploring the potential of Rayleigh-corrected reflectance in coastal and inland water applications: A simple aerosol correction method and its merits. *ISPRS Journal of Photogrammetry and Remote Sensing*, *146*, 52–64. doi:10.1016/j.isprsjprs.2018.08.020

Feng, L., Hou, X., & Zheng, Y. (2019). Monitoring and understanding the water transparency changes of fifty large lakes on the Yangtze Plain based on long-term MODIS observations. *Remote Sensing of Environment*, *221*, 675–686. doi:10.1016/j.rse.2018.12.007

Feng, L., Hu, C., Chen, X., & Song, Q. (2014). Influence of the three Gorges Dam on total suspended matters in the Yangtze Estuary and its adjacent coastal waters: Observations from MODIS. *Remote Sensing of Environment*, *140*, 779–788. doi:10.1016/j.rse.2013.10.002

Feng, L., Hu, C., Han, X., Chen, X., & Qi, L. (2014). Long-term distribution patterns of chlorophyll-a concentration in China's largest freshwater lake: MERIS full-resolution observations with a practical approach. *Remote Sensing*, *7*(1), 275–299. doi:10.3390/rs70100275

Fu, Y. Z., Xu, S. G., Zhang, C. K., & Sun, Y. (2018). Spatial downscaling of MODIS chlorophyll-a using Landsat 8 images for complex coastal water monitoring. *Estuarine Coastal and Shelf Science*, *209*, 149–159. doi:10.1016/j.ecss.2018.05.031

Gao, F., Li, J., Lin, H., & He, S. (2017). Oil pollution discrimination by an inelastic hyperspectral Scheimpflug lidar system. *Optics Express*, *25*(21), 25515–25522. doi:10.1364/OE.25.025515

Gao, Y., Jia, Y. L., Yu, G. R., He, N. P., Zhang, L., Zhu, B., & Wang, Y. F. (2019). Anthropogenic reactive nitrogen deposition and associated nutrient limitation effect on gross primary productivity in inland water of China. *Journal of Cleaner Production*, *208*(1), 530–540. doi:10.1016/j.jclepro.2018.10.137

Gao, Y. N., Gao, J. F., Yin, H. B., Liu, C. S., Xia, T., Wang, J., & Huang, Q. (2015). Remote sensing estimation of the total phosphorus concentration in a large lake using band combinations and regional multivariate statistical modeling techniques. *Journal of Environmental Management*, *151*, 33–43. doi:10.1016/j.jenvman.2014.11.036

Gong, P., Liang, S., Carlton, E. J., Jiang, Q., Wu, J., Wang, L., & Remais, J. V. (2012). Urbanisation and health in China. *Lancet (London, England)*, *379*(9818), 843–852. doi:10.1016/S0140-6736(11)61878-3

Gordon, H., & Morel, A. (1983). *Remote assessment of ocean color for interpretation of satellite visible imagery: A review. Lecture Notes on Coastal and Estuarine Studies*. Berlin, Germany: Springer Verlag.

Gordon, H. R., Clark, D. K., Brown, J. W., Brown, O. B., Evans, R. H., & Broenkow, W. W. (1983). Phytoplankton pigment concentrations in the Middle Atlantic Bight: Comparison of ship determinations and CZCS estimates. *Applied Optics*, *22*(1), 20–36. doi:10.1364/ao.22.000020

Guo, Q. Z., Wu, X. X., Bing, Q. X., Pan, Y. Y., Wang, Z. H., Fu, Y., … Liu, J. N. (2016). Study on retrieval of chlorophyll-a concentration based on Landsat OLI imagery in the Haihe River, China. *Sustainability*, *8*(8), 758. doi:10.3390/su8080758

Guo, Y. L., Li, Y. M., Zhu, L., Wang, Q., Lv, H., Huang, C. C., & Li, Y. (2016). An inversion-based fusion method for inland water remote monitoring. *IEEE Journal of Selected Topics in Applied Earth Observations and Remote Sensing*, *9*(12), 5599–5611. doi:10.1109/JSTARS.2016.2615125

Han, D., Currell, M. J., & Cao, G. (2016). Deep challenges for China's war on water pollution. *Environmental Pollution*, *218*, 1222–1233. doi:10.1016/j.envpol.2016.08.078

Han, Z., Jin, Y. Q., & Yun, C. X. (2006). Suspended sediment concentrations in the Yangtze River estuary retrieved from the CMODIS data. *International Journal of Remote Sensing*, *27*(19), 4329–4336. doi:10.1080/01431160600658164

Harmel, T., Chami, M., Tormos, T., Reynaud, N., & Danis, P. A. (2018). Sunglint correction of the multi-spectral instrument (MSI)-sentinel-2 imagery over inland and sea waters from SWIR bands. *Remote Sensing of Environment*, *204*, 308–321. doi:10.1016/j.rse.2017.10.022

He, W., Chen, S., Liu, X., & Chen, J. (2008). Water quality monitoring in a slightly-polluted inland water body through remote sensing—Case study of the Guanting Reservoir in Beijing. *Frontiers of Environmental Science & Engineering in China*, *2*(2), 163–171. doi:10.1007/s11783-008-0027-7

He, X. Q., Pan, D. L., & Zhu, Q. K. (2005). Exact Rayleigh scattering calculation for Chinese ocean color and temperature scanner. *Acta Optica Sinica*, *25*(2), 145–151.

He, X., Bai, Y., Wei, J., Ding, J., Shanmugam, P., Wang, D., … Huang, X. (2017). Ocean color retrieval from MWI onboard the Tiangong-2 space lab: Preliminary results. *Optics Express*, *25*(20), 23955–23973. doi:10.1364/OE.25.023955

Hollocher, K. (2002). Illustration gallery. Retrieved from http://minerva.union.edu/hollochk/kth/illustrations.html

Hou, Y., Li, Y., Liu, B., Liu, Y., & Wang, T. (2018). Design and implementation of a coastal-mounted sensor for oil film detection on seawater. *Sensors*, *18*(2), 70. doi:10.3390/s18010070

Hu, S., Zhou, W., Wang, G., Cao, W., Xu, Z., Liu, H., … Zhao, W. (2018). Comparison of satellite-derived phytoplankton size classes using in-situ measurements in the South China Sea. *Remote Sensing*, *10*(4), 526. doi:10.3390/rs10040526

Hu, S. B., Cao, W. X., Wang, G. F., Xu, Z. T., Lin, J. F., Zhao, W. J., … Yao, L. J. (2016). Comparison of MERIS, MODIS, SeaWiFS-derived particulate organic carbon, and in situ measurements in the South China Sea. *International Journal of Remote Sensing*, *37*(7), 1585–1600. doi:10.1080/01431161.2015.1088673

Huang, C. C., Jiang, Q. L., Yao, L., Li, Y. M., Yang, H., Huang, T., & Zhang, M. (2017). Spatiotemporal variation in particulate organic carbon based on long-term MODIS observations in Taihu Lake, China. *Remote Sensing*, *9*(6), 624. doi:10.3390/rs9060624

Huang, C. C., Li, Y. M., Liu, G., Guo, Y. L., Yang, H., Zhu, A. X., … Shi, K. (2017). Tracing high time-resolution fluctuations in dissolved organic carbon using satellite and buoy observations: Case study in Lake Taihu, China. *International Journal of Applied Earth Observation and Geoinformation*, *62*, 174–182. doi:10.1016/j.jag.2017.06.009

IOCCG. (1999). Status and plans for satellite ocean-colour missions: Considerations for complementary missions. In J. A. Yoder (Ed.). *Reports of the International Ocean-Colour Coordinating Group, No. 2*. Dartmouth, Canada: IOCCG.

IOCCG. (2000). Remote sensing of ocean colour in coastal, and other optically-complex, waters. In S. Sathyendranath (Ed.), *Reports of the International Ocean-Colour Coordinating Group, No. 3*. Dartmouth, Canada: IOCCG.

IOCCG. (2012). Mission requirements for future ocean-colour sensors. In C. R. McClain, and G. Meister (Eds.), *Reports of the International Ocean-Colour Coordinating Group, No. 13*. Dartmouth, Canada: IOCCG.

Jiang, Y. (2015). China's water security: Current status, emerging challenges, and future prospects. *Environmental Science & Policy*, *54*, 106–125. doi:10.1016/j.envsci.2015.06.006

Jin, Q., Lyu, H., Shi, L., Miao, S., Wu, Z. M., Li, Y. M., & Wang, Q. (2017). Developing a two-step method for retrieving cyanobacteria abundance from inland eutrophic lakes using MERIS data. *Ecological Indicators*, *81*, 543–554. doi:10.1016/j.ecolind.2017.06.027

Jin, S., Lu, Y. C., Liu, Y. X., Wei, X. L., Lu, W. Y., Wang, D. F., & Mao, Z. H. (2018). Refined use of AISA band-differences for oil slick identification beyond brightness contrast reversal under sunglint. *Optics Express*, *26*(26), 33748–33755. doi:10.1364/OE.26.033748

Kay, S., Hedley, J. D., & Lavender, S. (2009). Sun glint correction of high and low spatial resolution images of aquatic scenes: A review of methods for visible and near-infrared wavelengths. *Remote Sensing*, *1*(4), 697–730. doi:10.3390/rs1040697

Kokaly, R. F., Clark, R. N., Swayze, G. A., Livo, K. E., Hoefen, T. M., Pearson, N. C., … Klein, A. J. (2017). USGS Spectral Library Version 7: U.S. Geological Survey Data Series 1035. pp. 61. doi:10.3133/ds1035

Kong, J. L., Sun, X. M., Wang, W. K., Du, D., Chen, Y., & Yang, J. (2015). An optimal model for estimating suspended sediment concentration from Landsat TM images in the Caofeidian coastal waters. *International Journal of Remote Sensing*, *36*(19–20), 5257–5272. doi:10.1080/01431161.2015.1043159

Kutser, T., Vahtmäe, E., & Praks, J. (2009). A sun glint correction method for hyperspectral imagery containing areas with non-negligible water leaving NIR signal. *Remote Sensing of Environment*, *113*(10), 2267–2274. doi:10.1016/j.rse.2009.06.016

Le, C., Li, Y., Zha, Y., Sun, D., Huang, C., & Zhang, H. (2011). Remote estimation of chlorophyll a in optically complex waters based on optical classification. *Remote Sensing of Environment*, *115*(2), 725–737. doi:10.1016/j.rse.2010.10.014

Le, C. F., Li, Y. M., Zha, Y., Sun, D. Y., Huang, C. H., & Lu, H. (2009). A four-band semi-analytical model for estimating chlorophyll a in highly turbid lakes: The case of Taihu Lake, China. *Remote Sensing of Environment*, *113*(6), 1175–1182. doi:10.1016/j.rse.2009.02.005

Li, J., Hu, C., Shen, Q., Barnes, B. B., Murch, B., Feng, L., … Zhang, B. (2017). Recovering low quality MODIS-Terra data over highly turbid waters through noise reduction and regional vicarious calibration adjustment: A case study in Taihu Lake. *Remote Sensing of Environment*, *197*, 72–84. doi:10.1016/j.rse.2017.05.027

Li, Y., Zhang, Y. L., Shi, K., Zhou, Y. Q., Zhang, Y. B., Liu, X. H., & Guo, Y. L. (2018). Spatiotemporal dynamics of chlorophyll-a in a large reservoir as derived from Landsat 8 OLI data: Understanding its driving and restrictive factors. *Environmental Science and Pollution Research*, *25*(2), 1359–1374. doi:10.1007/s11356-017-0536-7

Li, Y., Zhang, Y. L., Shi, K., Zhu, G. W., Zhou, Y. Q., Zhang, Y. B., & Guo, Y. L. (2017). Monitoring spatiotemporal variations in nutrients in a large drinking water reservoir and their relationships with hydrological and meteorological conditions based on Landsat 8 imagery. *Science of the Total Environment*, *599*, 1705–1717. doi:10.1016/j.scitotenv.2017.05.075

Liang, S. (2004). *Quantitative remote sensing of land surfaces*. Hoboken, NJ: John Wiley and Sons, Inc.

Lin, J., Lyu, H., Miao, S., Pan, Y., Wu, Z. M., Li, Y. M., & Wang, Q. (2018). A two-step approach to mapping particulate organic carbon (POC) in inland water using OLCI images. *Ecological Indicators*, *90*, 502–512. doi:10.1016/j.ecolind.2018.03.044

Ling, Z. B., Sun, D. Y., Wang, S. Q., Qiu, Z. F., Huan, Y., Mao, Z. H., & He, Y. J. (2018). Retrievals of phytoplankton community structures from in situ fluorescence measurements by HS-6P. *Optics Express*, *26*(23), 30556–30575. doi:10.1364/OE.26.030556

Liu, B., Li, Y., Liu, C., Xie, F., & Muller, J.-P. (2018). Hyperspectral features of oil-polluted sea ice and the response to the contamination area fraction. *Sensors*, *18*(2), 234. doi:10.3390/s18010234

Liu, D., Bai, Y., He, X. Q., Pan, D. L., Wang, D. F., Wei, J. A., & Zhang, L. (2018). The dynamic observation of dissolved organic matter in the Zhujiang (Pearl River) Estuary in China from space. *Acta Oceanologica Sinica*, *37*(7), 105–117. doi:10.1007/s13131-017-1248-7

Liu, D. Z., Fu, D. Y., Xu, B., & Shen, C. Y. (2012). Estimation of total suspended matter in the Zhujiang (Pearl) River estuary from Hyperion imagery. *Chinese Journal of Oceanology and Limnology*, *30*(1), 16–21. doi:10.1007/s00343-012-0148-5

Liu, J., Liu, J. H., He, X. Q., Pan, D. L., Bai, Y., Zhu, F., … Wang, Y. (2018). Diurnal dynamics and seasonal variations of total suspended particulate matter in highly turbid Hangzhou Bay waters based on the geostationary ocean color imager. *IEEE Journal of Selected Topics in Applied Earth Observations and Remote Sensing*, *11*(7), 2170–2180. doi:10.1109/JSTARS.2018.2830335

Liu, J., & Yang, W. (2012). Water management. Water sustainability for China and beyond. *Science (New York, N.Y.)*, *337*(6095), 649–650. doi:10.1126/science.1219471

Liu, M., Merchant, C. J., Guan, L., & Mittaz, J. P. D. (2018). Inter-calibration of HY-1B/COCTS thermal infrared channels with MetOp-A/IASI. *Remote Sensing*, *10*(8), 1173. doi:10.3390/rs10081173

Liu, M. L., Liu, X. N., Li, J., Ding, C., & Jiang, J. L. (2014). Evaluating total inorganic nitrogen in coastal waters through fusion of multi-temporal RADARSAT-2 and optical imagery using random forest algorithm. *International Journal of Applied Earth Observation and Geoinformation*, *33*, 192–202. doi:10.1016/j.jag.2014.05.009

Lou, X., & Hu, C. (2014). Diurnal changes of a harmful algal bloom in the East China Sea: Observations from GOCI. *Remote Sensing of Environment*, *140*, 562–572. doi:10.1016/j.rse.2013.09.031

Lu, Y., Song, S., Wang, R., Liu, Z., Meng, J., Sweetman, A. J., … Luo, W. (2015). Impacts of soil and water pollution on food safety and health risks in China. *Environment International*, *77*, 5–15. doi:10.1016/j.envint.2014.12.010

Lu, Y., Yuan, J., Lu, X., Su, C., Zhang, Y., Wang, C., … Sweijd, N. (2018). Major threats of pollution and climate change to global coastal ecosystems and enhanced management for sustainability. *Environmental Pollution (Barking, Essex : 1987)*, *239*, 670–680. doi:10.1016/j.envpol.2018.04.016

Lyu, H., Wang, Y. N., Jin, Q., Li, X. J., Cao, K., Wang, Q. A., & Li, Y. M. (2017). A practical approach to retrieving the finer areas of algal bloom in inland lakes from coarse spatial resolution satellite data. *International Journal of Remote Sensing*, *38*(14), 4069–4085. doi:10.1080/01431161.2017.1312621

Lyu, H., Wang, Y. N., Jin, Q., Shi, L., Li, Y. M., & Wang, Q. (2017). Developing a semi-analytical algorithm to estimate particulate organic carbon (POC) levels in inland eutrophic turbid water based on MERIS images: A case study of Lake Taihu. *International Journal of Applied Earth Observation and Geoinformation*, *62*, 69–77. doi:10.1016/j.jag.2017.06.001

Mao, Y., Wang, S. Q., Qiu, Z. F., Sun, D. Y., & Bilal, M. (2018). Variations of transparency derived from GOCI in the Bohai Sea and the Yellow Sea. *Optics Express*, *26*(9), 12191–12209.

Mao, Z. H., Chen, J. Y., Pan, D. L., Tao, B. Y., & Zhu, Q. K. (2012). A regional remote sensing algorithm for total suspended matter in the East China Sea. *Remote Sensing of Environment*, *124*, 819–831. doi:10.1016/j.rse.2012.06.014

Mao, Z. H., Zhu, Q. K., & Gong, F. (2007). The algorithms of chlorophyll-a concentration for CMODIS. *Acta Oceanologica Sinica*, *26*(5), 25–33.

Martin, J., Eugenio, F., Marcello, J., & Medina, A. (2016). Automatic sun glint removal of multispectral high-resolution WorldView-2 imagery for retrieving coastal shallow water parameters. *Remote Sensing*, *8*(1), 37. doi:10.3390/rs8010037

Matthews, M. W. (2011). A current review of empirical procedures of remote sensing in inland and near-coastal transitional waters. *International Journal of Remote Sensing*, *32*(21), 6855–6899. doi:10.1080/01431161.2010.512947

Ministry of Environmental Protection of the People's Republic of China (MEP). (1997). Sea water quality standard (GB 3097-1997) (in Chinese). Retrieved from http://english.mee.gov.cn/Resources/standards/water_environment/quality_standard/200710/t20071024_111791.shtml

Ministry of Environmental Protection of the People's Republic of China (MEP). (2002). Environmental quality standards for surface water (GB 3838-2002) (in Chinese). Retrieved from http://english.mee.gov.cn/Resources/standards/water_environment/quality_standard/200710/t20071024_111792.shtml

Ministry of Environmental Protection of the People's Republic of China (MEP). (2008). Specifications for environmental monitoring in coastal sea areas (HJ 442-2008) (in Chinese). Retrieved from http://english.mee.gov.cn/News_service/Photo/200907/t20090714_155177.shtml

Ministry of Housing and Urban-Rural Development of the People's Republic of China (MOHURD). (2017). The 13th five-year plan for construction of National Urban Municipal Infrastructure (in Chinese).

Ministry of Water Resources of the People's Republic of China (MWR) and National Bureau of Statistics of the People's Republic of China (NBS). (2013). *Bulletin of first National Census for Water*. Beijing, China: China Water & Power Press.

Mouw, C. B., Greb, S., Aurin, D., DiGiacomo, P. M., Lee, Z., Twardowski, M., … Craig, S. E. (2015). Aquatic color radiometry remote sensing of coastal and inland waters: Challenges and recommendations for future satellite missions. *Remote Sensing of Environment*, *160*, 15–30. doi:10.1016/j.rse.2015.02.001

Nazeer, M., & Nichol, J. E. (2016a). Development and application of a remote sensing-based chlorophyll-a concentration prediction model for complex coastal waters of Hong Kong. *Journal of Hydrology*, *532*, 80–89. doi:10.1016/j.jhydrol.2015.11.037

Nazeer, M., & Nichol, J. E. (2016b). Improved water quality retrieval by identifying optically unique water classes. *Journal of Hydrology*, *541*, 1119–1132. doi:10.1016/j.jhydrol.2016.08.020

Odermatt, D., Gitelson, A., Brando, V. E., & Schaepman, M. (2012). Review of constituent retrieval in optically deep and complex waters from satellite imagery. *Remote Sensing of Environment*, *118*, 116–126. doi:10.1016/j.rse.2011.11.013

Ogashawara, I. (2015). Terminology and classification of bio-optical models. *Remote Sensing Letters*, *6*(8), 613–617. doi:10.1080/2150704X.2015.1066523

Ogashawara, I., Mishra, D. R., & Gitelson, A. A. (2017). Remote sensing of inland waters: Background and current state-of-the-art. In D. R. Mishra, I. Ogashawara, & A. A. Gitelson (Eds.), *Bio-optical modeling and remote sensing of inland waters* (1st ed., pp. 332). New York, NY: Elsevier.

Oki, T., & Kanae, S. (2006). Global hydrological cycles and world water resources. *Science (New York, N.Y.)*, *313*(5790), 1068–1072. doi:10.1126/science.1128845

Paerl, H. W., & Huisman, J. (2009). Climate change: A catalyst for global expansion of harmful cyanobacterial blooms. *Environmental Microbiology Reports*, *1*(1), 27–37. doi:10.1111/j.1758-2229.2008.00004.x

Pahlevan, N., Chittimalli, S. K., Balasubramanian, S. V., & Vellucci, V. (2019). Sentinel-2/Landsat-8 product consistency and implications for monitoring aquatic systems. *Remote Sensing of Environment*, *220*, 19–29. doi:10.1016/j.rse.2018.10.027

Palmer, S. C., Kutser, T., & Hunter, P. D. (2015). Remote sensing of inland waters: Challenges, progress and future directions. *Remote Sensing of Environment*, *157*(2), 1–8. doi:10.1016/j.rse.2014.09.021

Pan, D., He, X., & Zhu, Q. (2004). On orbit cross-calibration of HY-1A satellite sensor COCTS. *Chinese Science Bulletin*, *49*(23), 2521–2244. doi:10.1360/04wd0057

Pan, D. L., He, X. Q., & Mao, T. (2003). Preliminary study on the orbit cross-calibration of CMODIS by SeaWiFS. *Progress in Natural Science*, *10*, 745–749. doi:10.1080/10020070312331344350

Pan, Y. Q., Shen, F., & Wei, X. D. (2018). Fusion of Landsat-8/OLI and GOCI data for hourly mapping of suspended particulate matter at high spatial resolution: A case study in the Yangtze (Changjiang) Estuary. *Remote Sensing*, *10*(2), 158. doi:10.3390/rs10020158

Peking University Center for Legal Information. (2017). Water pollution prevention and control law of the People's Republic of China (2017 Revision). Retrieved from http://en.pkulaw.cn/display.aspx?cgid=297378&lib=law

Qi, L., Hu, C., Duan, H., Cannizzaro, J., & Ma, R. (2014). A novel MERIS algorithm to derive cyanobacterial phycocyanin pigment concentrations in a eutrophic lake:

Theoretical basis and practical considerations. *Remote Sensing of Environment*, *154*, 298–317. doi:10.1016/j.rse.2014.08.026

Qi, L., Hu, C., Visser, P. M., & Ma, R. (2018). Diurnal changes of cyanobacteria blooms in Taihu Lake as derived from GOCI observations. *Limnology and Oceanography*, *63*(4), 1711–1726. doi:10.1002/lno.10802

Qiu, Z. F., Xiao, C., Perrie, W., Sun, D. Y., Wang, S. Q., Shen, H., … He, Y. J. (2017). Using Landsat 8 data to estimate suspended particulate matter in the Yellow River estuary. *Journal of Geophysical Research: Oceans*, *122*(1), 276–290. doi:10.1002/2016JC012412

Ren, J. L., Zheng, Z. B., Li, Y. M., Lv, G. N., Wang, Q., Lyu, H., … Bi, S. (2018). Remote observation of water clarity patterns in Three Gorges Reservoir and Dongting Lake of China and their probable linkage to the Three Gorges Dam based on Landsat 8 imagery. *Science of the Total Environment*, *625*, 1554–1566. doi:10.1016/j.scitotenv.2018.01.036

Schmugge, T. J., Kustas, W. P., Ritchie, J. C., Jackson, T. J., & Rango, A. (2002). Remote sensing in hydrology. *Advances in Water Resources*, *25*(8–12), 1367–1385. doi:10.1016/S0309-1708(02)00065-9

Shang, S., Lee, Z., Lin, G., Hu, C., Shi, L., Zhang, Y., … Yan, J. (2017). Sensing an intense phytoplankton bloom in the western Taiwan Strait from radiometric measurements on a UAV. *Remote Sensing of Environment*, *198*, 85–94. doi:10.1016/j.rse.2017.05.036

Shanmugam, P., He, X. Q., Singh, R. K., & Varunan, T. (2018). A modern robust approach to remotely estimate chlorophyll in coastal and inland zones. *Advances in Space Research*, *61*(10), 2491–2509. doi:10.1016/j.asr.2018.02.024

Shen, L., Xu, H., & Guo, X. (2012). Satellite remote sensing of harmful algal blooms (HABs) and a potential synthesized framework. *Sensors*, *12*(6), 7778–7803. doi:10.3390/s120607778

Shen, X., & Feng, Q. (2018). Statistical model and estimation of inland riverine turbidity with Landsat 8 OLI images: A case study. *Environmental Engineering Science*, *35*(2), 132–140. doi:10.1089/ees.2016.0540

Shi, K., Li, Y., Li, L., Lu, H., Song, K., Liu, Z., … Li, Z. (2013). Remote chlorophyll-a estimates for inland waters based on a cluster-based classification. *Science of the Total Environment*, *444*, 1–15. doi:10.1016/j.scitotenv.2012.11.058

Shi, K., Zhang, Y. L., Li, Y. M., Li, L., Lv, H., & Liu, X. H. (2015). Remote estimation of cyanobacteria-dominance in inland waters. *Water Research*, *68*, 217–226. doi:10.1016/j.watres.2014.10.019

Shi, W., Zhang, Y. L., & Wang, M. H. (2018). Deriving total suspended matter concentration from the near-infrared-based inherent optical properties over turbid waters: A case study in Lake Taihu. *Remote Sensing*, *10*(2), 333. doi:10.3390/rs10020333

Shi, Z. H., Yu, L., Cao, D. S., Wu, Q. W., Yu, X. Y., & Lin, G. Y. (2015). Airborne ultraviolet imaging system for oil slick surveillance: Oil–seawater contrast, imaging concept, signal-to-noise ratio, optical design, and optomechanical model. *Applied Optics*, *54*(25), 7648–7655. doi:10.1364/AO.54.007648

Siswanto, E., Tang, J., Yamaguchi, H., Ahn, Y. H., Ishizaka, J., Yoo, S., … Kawamura, H. (2011). Empirical ocean-color algorithms to retrieve chlorophyll-a, total suspended matter, and colored dissolved organic matter absorption coefficient in the Yellow and East China Seas. *Journal of oceanography*, *67*(5), 627–650.

Son, Y. B., Choi, B. J., Kim, Y. H., & Park, Y. G. (2015). Tracing floating green algae blooms in the Yellow Sea and the East China Sea using GOCI satellite data and Lagrangian transport simulations. *Remote Sensing of Environment*, *156*, 21–33. doi:10.1016/j.rse.2014.09.024

Song, K., Li, L., Tedesco, L. P., Li, S., Duan, H., Liu, D., Hall, B. E., … Zhao, Y. (2013). Remote estimation of chlorophyll-a in turbid inland waters: Three-band model versus GA-PLS model. *Remote Sensing of Environment*, *136*, 342–357. doi:10.1016/j.rse.2013.05.017

Suif, Z., Fleifle, A., Yoshimura, C., & Saavedra, O. (2016). Spatio-temporal patterns of soil erosion and suspended sediment dynamics in the Mekong River Basin. *The Science of the Total Environment*, *568*, 933–945. doi:10.1016/j.scitotenv.2015.12.134

Sun, D., Hu, C., Qiu, Z., & Shi, K. (2015). Estimating phycocyanin pigment concentration in productive inland waters using Landsat measurements: A case study in Lake Dianchi. *Optics Express*, *23*(3), 3055–3074. doi:10.1364/OE.23.003055

Sun, S., Lu, Y., Liu, Y., Wang, M., & Hu, C. (2018). Tracking an oil tanker collision and spilled oils in the East China Sea using multisensor day and night satellite imagery. *Geophysical Research Letters*, *45*(7), 3212–3220. doi:10.1002/2018GL077433

Sun, X., Shen, F., Liu, D., Bellerby, R. G. J., Liu, Y., & Tang, R. (2018). In situ and satellite observations of phytoplankton size classes in the entire continental shelf sea, China. *Journal of Geophysical Research: Oceans*, *123*, 3523–3544. doi:10.1029/2017JC013651

Sun, X., Wu, M. Q., Xing, Q. G., Song, X. D., Zhao, D. H., Han, Q. Q., & Zhang, G. Z. (2018). Spatio-temporal patterns of Ulva prolifera blooms and the corresponding influence on chlorophyll-a concentration in the Southern Yellow Sea, China. *Science of the Total Environment*, *640*, 807–820. doi:10.1016/j.scitotenv.2018.05.378

Tang, D. L., Ni, I. H., Muller-Karger, F. E., & Oh, I. S. (2004). Monthly variation of pigment concentrations and seasonal winds in China's marginal seas. *Hydrobiologia*, *511*(1), 1–15. doi:10.1023/B:HYDR.0000014001.43554.6f

Tao, B. Y., Mao, Z. H., Lei, H., Pan, D. L., Bai, Y., Zhu, Q. K., & Zhang, Z. L. (2017). A semianalytical MERIS green-red band algorithm for identifying phytoplankton bloom types in the East China Sea. *Journal of Geophysical Research: Oceans*, *122*(3), 1772–1788. doi:10.1002/2016JC012368

Tao, B., Mao, Z., Lei, H., Pan, D., Shen, Y., Bai, Y., … Li, Z. (2015). A novel method for discriminating Prorocentrum donghaiense from diatom blooms in the East China Sea using MODIS measurements. *Remote Sensing of Environment*, *158*, 267–280. doi:10.1016/j.rse.2014.11.004

Tao, T., & Xin, K. (2014). Public health: A sustainable plan for China's drinking water. *Nature*, *511*(7511), 527–528. doi:10.1038/511527a

The State Council. (2015, April 16). China announces action plan to tackle water pollution. Retrieved from http://english.gov.cn/policies/latest_releases/2015/04/16/content_281475090170164.htm

The State Council. (2018, June 24). China unveils guideline to win battle against pollution. Retrieved from http://english.gov.cn/policies/latest_releases/2018/06/24/content_281476197094344.htm

Tian, H., Cao, C., Xu, M., Zhu, Z., Liu, D., Wang, X., & Cui, S. (2014). Estimation of chlorophyll-a concentration in coastal waters with HJ-1A HSI data using a three-band bio-optical model and validation. *International Journal of Remote Sensing*, *35*(16), 5984–6003. doi:10.1080/01431161.2014.934403

Tian, L. Q., Wai, O. W. H., Chen, X. L., Li, W. B., Li, J., Li, W. K., & Zhang, H. D. (2016). Retrieval of total suspended matter concentration from Gaofen-1 Wide Field Imager (WFI) multispectral imagery with the assistance of Terra MODIS in turbid water-case in Deep Bay. *International Journal of Remote Sensing*, *37*(14), 3400–3413. doi:10.1080/01431161.2016.1199084

Tian, L. Q., Wai, O. W. H., Chen, X. L., Liu, Y. H., Feng, L., Li, J., & Huang, J. (2014). Assessment of total suspended sediment distribution under varying tidal conditions in deep bay: Initial results from HJ-1A/1B satellite CCD images. *Remote Sensing*, *6*(10), 9911–9929. doi:10.3390/rs6109911

Van Dijk, A. I. J. M., Beck, H. E., Crosbie, R. S., De Jeu, R. A. M., Liu, Y. Y., Podger, G. M., … Viney, N. R. (2013). The millennium drought in southeast Australia (2001–2009): Natural and human causes and implications for water resources, ecosystems, economy, and society. *Water Resources Research*, *49*(2), 1040–1057. doi:10.1002/wrcr.20123

Vörösmarty, C. J., McIntyre, P., Gessner, M., Dudgeon, D., Prusevich, A., Green, P. … Davies, P. M. (2010). Global threats to human water security and river biodiversity. *Nature*, *467*(7315), 555–561. doi:10.1038/nature09440

Wada, Y., Wisser, D., & Bierkens, M. F. P. (2014). Global modeling of withdrawal, allocation and consumptive use of surface water and groundwater resources. *Earth System Dynamics*, *5*(1), 15–40. doi:10.5194/esd-5-15-2014

Wang, C. Y., Chen, S. S., Li, D., Wang, D. N., Liu, W., & Yang, J. (2017). A Landsat-based model for retrieving total suspended solids concentration of estuaries and coasts in China. *Geoscientific Model Development*, *10*(12), 4347–4365. doi:10.5194/gmd-10-4347-2017

Wang, J., Li, L., Li, F., Kharrazi, A., & Bai, Y. (2018). Regional footprints and interregional interactions of chemical oxygen demand discharges in China. *Resources Conservation and Recyling*, *132*, 386–397. doi:10.1016/j.resconrec.2017.08.008

Wang, J. J., & Lu, X. X. (2010). Estimation of suspended sediment concentrations using Terra MODIS: An example from the Lower Yangtze River, China. *The Science of the Total Environment*, *408*(5), 1131–1138. doi:10.1016/j.scitotenv.2009.11.057

Wang, J. J., Lu, X. X., Liew, S. C., & Zhou, Y. (2009). Retrieval of suspended sediment concentrations in large turbid rivers using Landsat ETM+: An example from the Yangtze River, China. *Earth Surface Processes and Landforms*, *34*(8), 1082–1092. doi:10.1002/esp.1795

Wang, M., & Shi, W. (2007). The NIR-SWIR combined atmospheric correction approach for MODIS ocean color data processing. *Optics Express*, *15*(24), 15722–15733. doi:10.1364/oe.15.015722

Wang, M., Shi, W., & Tang, J. (2011). Water property monitoring and assessment for China's inland Taihu Lake from MODIS-Aqua measurements. *Remote Sensing of Environment*, *115*(3), 841–854. doi:10.1016/j.rse.2010.11.012

Wang, X., Gong, Z. N., & Pu, R. L. (2018). Estimation of chlorophyll a content in inland turbidity waters using WorldView-2 imagery: A case study of the Guanting Reservoir, Beijing, China. *Environmental Monitoring and Assessment*, *190*(10), 620. doi:10.1007/s10661-018-6978-7

Wang, X., & Ma, T. (2001). Application of remote sensing techniques in monitoring and assessing the water quality of Taihu Lake. *Bulletin of Environmental Contamination and Toxicology*, *67*(6), 863–870. doi:10.1007/s001280202

Wang, Y. C., Shen, F., Sokoletsky, L., & Sun, X. (2017). Validation and calibration of QAA algorithm for CDOM absorption retrieval in the Changjiang (Yangtze) Estuarine and Coastal Waters. *Remote Sensing*, *9*(11), 1192. doi:10.3390/rs9111192

Wang, Y. P., Xia, H., Fu, J. M., & Sheng, G. Y. (2004). Water quality change in reservoirs of Shenzhen, China: Detection using LANDSAT/TM data. *Science of the Total Environment*, *328*(1–3), 195–206. doi:10.1016/j.scitotenv.2004.02.020

Wu, G. F., Cui, L. J., He, J. J., Duan, H. T., Fei, T., & Liu, Y. L. (2013). Comparison of MODIS-based models for retrieving suspended particulate matter concentrations in Poyang Lake, China. *International Journal of Applied Earth Observation and Geoinformation*, *24*, 63–72. doi:10.1016/j.jag.2013.03.001

Wu, G. F., Liu, L. J., Chen, F. Y., & Fei, T. (2014). Developing MODIS-based retrieval models of suspended particulate matter concentration in Dongting Lake, China. *International Journal of Applied Earth Observation and Geoinformation*, *32*, 46–53. doi:10.1016/j.jag.2014.03.025

Wu, X., Duan, H. Q., Bi, N. S., Yuan, P., Wang, A. M., & Wang, H. J. (2016). Interannual and seasonal variation of chlorophyll-a off the Yellow River Mouth (1997–2012): Dominance of river inputs and coastal dynamics. *Estuarine Coastal and Shelf Science*, *183*, 402–412. doi:10.1016/j.ecss.2016.08.038

Xing, Q. G., & Hu, C. M. (2016). Mapping macroalgal blooms in the Yellow Sea and East China Sea using HJ-1 and Landsat data: Application of a virtual baseline reflectance height technique. *Remote Sensing of Environment*, *178*, 113–126. doi:10.1016/j.rse.2016.02.065

Xing, Q. G., Lou, M. J., Chen, C. Q., & Shi, P. (2013). Using in situ and Satellite Hyperspectral Data to Estimate the Surface Suspended Sediments Concentrations in the Pearl River Estuary. *Ieee Journal of Selected Topics in Applied Earth Observations and Remote Sensing*, *6*(2), 731–738. doi:10.1109/JSTARS.2013.2238659

Xinhua News. (2018a, May 8). China sends supervisors to inspect urban water pollution control. Retrieved from http://www.xinhuanet.com/english/2018-05/08/c_137162195.htm

Xinhua News. (2018b, December 1). China sends supervisors to inspect urban water pollution control. Retrieved from http://www.xinhuanet.com/english/2018-12/01/c_137644555.htm

Xiong, S., Long, H., Tang, G., Wan, J., & Li, H. (2015). The management in response to marine oil spill from ships in China: A systematic review. *Marine Pollution Bulletin*, *96*(1–2), 7–17. doi:10.1016/j.marpolbul.2015.05.027

Xu, F., Gao, Z., Jiang, X., Shang, W., Ning, J., Song, D., & Ai, J. (2018). A UAV and S2A data-based estimation of the initial biomass of green algae in the South Yellow Sea. *Marine Pollution Bulletin*, *128*, 408–414. doi:10.1016/j.marpolbul.2018.01.061

Xu, J., Fang, C. Y., Gao, D., Zhang, H. S., Gao, C., Xu, Z. C., & Wang, Y. Q. (2018). Optical models for remote sensing of chromophoric dissolved organic matter (CDOM) absorption in Poyang Lake. *ISPRS Journal of Photogrammetry and Remote Sensing*, *142*, 124–136. doi:10.1016/j.isprsjprs.2018.06.004

Xu, K., Milliman, J. D., & Xu, H. (2010). Temporal trend of precipitation and runoff in major Chinese rivers since 1951. *Global and Planetary Change*, *73*(3–4), 219–232. doi:10.1016/j.gloplacha.2010.07.002

Xu, Q., Li, X. F., Wei, Y. L., Tang, Z. Y., Cheng, Y. C., & Pichel, W. G. (2013). Satellite observations and modeling of oil spill trajectories in the Bohai Sea. *Marine Pollution Bulletin*, *71*(1–2), 107–116. doi:10.1016/j.marpolbul.2013.03.028

Xu, X., Huang, X. L., Zhang, Y. L., & Yu, D. (2018). Long-term changes in water clarity in Lake Liangzi determined by remote sensing. *Remote Sensing*, *10*(9), 1441. doi:10.3390/rs10091441

Xu, X. H., Pan, D. L., Mao, Z. H., & Tao, B. Y. (2014). A new algorithm based on the background field for red tide monitoring in the East China Sea. *Acta Oceanologica Sinica*, *33*(5), 62–71. doi:10.1007/s13131-014-0404-y

Yan, J., Wang, L., Chen, L., Zhao, L., & Huang, B. (2015). A dynamic remote sensing data-driven approach for oil spill simulation in the sea. *Remote Sensing*, *7*(6), 7105–7125. doi:10.3390/rs70607105

Yang, W., Matsushita, B., Chen, J., & Fukushima, T. (2011). Estimating constituent concentrations in case II waters from MERIS satellite data by semi-analytical model optimizing and look-up tables. *Remote Sensing of Environment*, *115*(5), 1247–1259. doi:10.1016/j.rse.2011.01.007

Yu, X., Yi, H. P., Liu, X. Y., Wang, Y. B., Liu, X., & Zhang, H. (2016). Remote-sensing estimation of dissolved inorganic nitrogen concentration in the Bohai Sea using band combinations derived from MODIS data. *International Journal of Remote Sensing*, *37*(2), 327–340. doi:10.1080/01431161.2015.1125555

Zhan, W. K., Wu, J., Wei, X., Tang, S. L., & Zhan, H. G. (2019). Spatio-temporal variation of the suspended sediment concentration in the Pearl River Estuary observed by MODIS during 2003-2015. *Continental Shelf Research*, *172*, 22–32. doi:10.1016/j.csr.2018.11.007

Zhang, F., Li, J., Shen, Q., Zhang, B., Wu, C., Wu, Y., … Lu, Z. (2015). Algorithms and schemes for chlorophyll a estimation by remote sensing and optical classification for Turbid Lake Taihu, China. *IEEE Journal of Selected Topics in Applied Earth Observations and Remote Sensing*, *8*(1), 350–364. doi:10.1109/JSTARS.2014.2333540

Zhang, F. F., Li, J. S., Shen, Q., Zhang, B., Tian, L. Q., Ye, H. P., … Lu, Z. Y. (2019). A soft-classification-based chlorophyll-a estimation method using MERIS data in the highly turbid and eutrophic Taihu Lake. *International Journal of Applied Earth Observation and Geoinformation*, *74*, 138–149. doi:10.1016/j.jag.2018.07.018

Zhang, G. Q., Yao, T. D., Xie, H. J., Qin, J., Ye, Q. H., Dai, Y. F., & Guo, R. F. (2014). Estimating surface temperature changes of lakes in the Tibetan Plateau using MODIS LST data. *Journal of Geophysical Research: Atmospheres*, *119*(14), 8552–8567. doi:10.1002/2014JD021615

Zhang, H., Wang, S., Qiu, Z., Sun, D., Ishizaka, J., Sun, S., & He, Y. (2018). Phytoplankton size class in the East China Sea derived from MODIS satellite data. *Biogeosciences*, *15*(13), 4271–4289. doi:10.5194/bg-15-4271-2018

Zhang, H. L., Qiu, Z. F., Sun, D. Y., Wang, S. Q., & He, Y. J. (2017). Seasonal and interannual variability of satellite-derived chlorophyll-a (2000–2012) in the Bohai Sea, China. *Remote Sensing*, *9*(6), 582. doi:10.3390/rs9060582

Zhang, J., Mauzerall, D., Zhu, T., Liang, S., Ezzati, M., & Remais, J. V. (2010). Environmental health in China: Progress towards clean air and safe water. *Lancet (London, England)*, *375*(9720), 1110–1119. doi:10.1016/S0140-6736(10)60062-1

Zhang, M., Shi, X., Yang, Z., Yu, Y., Shi, L., & Qin, B. (2018). Long-term dynamics and drivers of phytoplankton biomass in eutrophic Lake Taihu. *The Science of the Total Environment*, *645*, 876–886. doi:10.1016/j.scitotenv.2018.07.220

Zhang, M. W., Dong, Q., Cui, T. W., Xue, C. J., & Zhang, S. L. (2014). Suspended sediment monitoring and assessment for Yellow River estuary from Landsat TM and ETM plus imagery. *Remote Sensing of Environment*, *146*, 136–147. doi:10.1016/j.rse.2013.09.033

Zhang, Y. C., Ma, R. H., Zhang, M., Duan, H. T., Loiselle, S., & Xu, J. (2015). Fourteen-year record (2000–2013) of the spatial and temporal dynamics of floating algae blooms in Lake Chaohu, observed from time series of MODIS images. *Remote Sensing*, *7*(8), 10523–10542. doi:10.3390/rs70810523

Zhang, Y. Z., Martti, H., Zhang, H. S., Duan, H. T., Li, Y., & Liang, X. S. (2018). Chlorophyll-a estimation in turbid waters using combined SAR data with hyperspectral reflectance data: A case study in Lake Taihu, China. *IEEE Journal of Selected Topics in Applied Earth Observations and Remote Sensing*, *11*(4), 1325–1336. doi:10.1109/JSTARS.2017.2789247

Zhao, D. Z., Zhao, L., Zhang, F. S., & Zhang, X. Y. (2004). Temporal occurrence and spatial distribution of red tide events in China's coastal waters. *Human and Ecological Risk Assessment: An International Journal*, *10*(5), 945–957. doi:10.1080/10807030490889030

Zhao, J., & Cao, W. X. (2012). First attempt to derive chlorophyll-a using natural fluorescence in Northern South China Sea. *Remote Sensing Letters*, *3*(3), 249–258. doi:10.1080/01431161.2011.566286

Zhao, J., Cao, W. X., Xu, Z. T., Ye, H. B., Yang, Y. Z., Wang, G. F., … Sun, Z. H. (2018). Estimation of suspended particulate matter in turbid coastal waters: Application to hyperspectral satellite imagery. *Optics Express*, *26*(8), 10476–10493. doi:10.1364/OE.26.010476

Zhao, S. H., Wang, Q., Li, Y., Liu, S. H., Wang, Z. T., Zhu, L., & Wang, Z. F. (2017). An overview of satellite remote sensing technology used in China's environmental protection. *Earth Science Informatics*, *10*(2), 137–148. doi:10.1007/s12145-017-0286-6

Zheng, G., & DiGiacomo, P. M. (2017). Uncertainties and applications of satellite-derived coastal water quality products. *Progress in Oceanography*, *159*, 45–72. doi:10.1016/j.pocean.2017.08.007

Zhou, B. T., Shang, M. S., Wang, G. Y., Feng, L., Shan, K., Liu, X. N., … Zhang, X. (2017). R. Remote estimation of cyanobacterial blooms using the risky grade index (RGI) and coverage area index (CAI): A case study in the Three Gorges Reservoir, China. *Environmental Science and Pollution Research*, *24*(23), 19044–19056. doi:10.1007/s11356-017-9544-x

Zhou, Q., Tian, L., Li, J., Song, Q., & Li, W. (2018). Radiometric cross-calibration of Tiangong-2 MWI visible/NIR channels over aquatic environments using MODIS. *Remote Sensing*, *10*(11), 1803. doi:10.3390/rs10111803

Zhu, Q., Li, J. S., Zhang, F. F., & Shen, Q. (2018). Distinguishing cyanobacterial bloom from floating leaf vegetation in Lake Taihu Based on medium-resolution imaging spectrometer (MERIS) data. *IEEE Journal of Selected Topics in Applied Earth Observations and Remote Sensing*, *11*(1), 34–44. doi:10.1109/JSTARS.2017.2757006

Appendix A

Table A1. Water quality standards in China.

Surface water: GB3838-2002		Coastal and sea water: GB3097-1997 and HJ 442-2008	
Grade	Applicability or uses	Grade	Applicability or uses
I	River headwaters and protected natural headwater areas	I	Protected natural sea water areas
II	First class water source protection areas for centralized drinking supply	II	Sea water areas with direct human contact or suitable for aquaculture
III	Second class water source protection areas for drinking supply and recreation	III	Industrial water supply and recreational water
IV	Industrial water supply and recreational water with no direct human contact	IV	Development zone, e.g. coastal port
V	Limited agricultural water supply		
Inferior to V	Unsafe for any use	Inferior to IV	Unsafe for any use

Source: Ministry of Environmental Protection (MEP, 1997, 2002, 2008).

Table A2. Summary of abbreviations and their definitions.

Abbreviation		Definition	Abbreviation		Definition
Water	AOPs	Apparent Optical Properties	Sensors	AISA	Airborne Imaging Spectrometer for Applications
quality	IOPs	Inherent Optical Properties		CCD	Charge-coupled Device
indices	K_d	Attenuation Coefficient		CMODIS	Chinese Moderate Resolution Imaging Spectroradiometer
	R_{rs}	Spectral Reflectance		CZCS	Coastal Zone Color Scanner
	CDOM	Colored Dissolved Organic Matter		ETM+	Enhanced Thematic Mapper
	Chla	Chlorophyll Concentration		GOCI	Geostationary Ocean Color Imager
	CSI	Chlorophyll spectral index		HICO	Hyperspectral Imager for the Coastal Ocean
	DOC	Dissolved Organic Carbon		MERIS	Medium Resolution Imaging Spectrometer
	FAH	Floatingmacro Algae Height		MODIS	Moderate Resolution Imaging Spectroradiometer
	FAI	Floating Algal Index		MSI	Multi-Spectral Instrument
	FLH	Fluorescence line height		OLCI	Ocean and Land Color Instrument
	AFAI	Adjusted Floating Algal Index		OLI	Operational Land Imager
	GABI	Generalized Algal Bloom index		PMS	Panchromatic and Multispectral Sensor
	IGAG	Index of floating Green Algae for GOCI		SeaWiFs	Sea-viewing Wide Field-of-view Sensor
	PC	Phycocyanin Pigment Concentration		TIRS	Thermal Infrared Sensor
	PCI	phycocyanin index		TM	Thematic Mapper
	POC	Particulate Organic Carbon		VIIRS	Visible Infrared Imager Radiometer Suite
	SAI	Spectral absorption index		WFV	Wide Field of View
	SPM	Suspended Particulate Matter		WV-2	Worldview 2
	SS	Suspended Solids	Spectral bands	MIR	Mid-Infrared
	SSC	Suspended Sediment Concentration		NIR	Near-Infrared
	SST	Sea Surface Temperature		SWIR	Shortwave Infrared
	TIN	Total Inorganic Nitrogen		TIR	Thermal Infrared
	TIP	Total Inorganic Phosphorus		UV	Ultraviolet
	TN	Total Nitrogen	Others	ANN	Artificial neural network
	TP	Total Phosphorus		NTU	Nephelometric turbidity units
	TSM	Total Suspended Matter			
	TSS	Total Suspended Solids			
	Z_{SD}	Secchi Disk Depth			